OILY MOLECULE HYDRATION-SHELL: THE INFLUENCE OF CROWDING, ELECTROLYTES AND SMALL MOLECULES

by

Aria J. Bredt

A Dissertation

Submitted to the Faculty of Purdue University

In Partial Fulfillment of the Requirements for the degree of

Doctor of Philosophy

Department of Chemistry

West Lafayette, Indiana

May 2021

THE PURDUE UNIVERSITY GRADUATE SCHOOL

STATEMENT OF COMMITTEE APPROVAL

Dr. Dor Ben-Amotz, Chair

Department of Chemistry

Dr. Garth Simpson

Department of Chemistry

Dr. Christopher Uyeda

Department of Chemistry

Dr. Lynne Taylor

Department of Industrial and Physical Pharmacy

Approved by:

Dr. Christine Hrycyna

To my parents, Ofelia and Paul, and brother, Jack

ACKNOWLEDGMENTS

I would like to acknowledge my family and friends for their continued support and reassurance throughout this process. Including Angela Donajkowski, who was willing to listen to multiple practice presentations throughout this journey and Gail Feldstein who was willing to read this dissertation and provide grammatical feedback.

I am happy to have completed my research in such a wonderful lab. As such, I would like to thank my advisor, Dr. Dor Ben-Amotz, for fostering a great atmosphere, his invaluable guidance and scientific knowledge. I would also like to acknowledge past and present Ben-Amotz group members. Louis Streacker for his mentorship when I first entered the lab. Dr. Sarah Matt, Dr. Shannon Pattenaude, and Colby Raymond who were allows willing to lend an ear as well as Patrick Wise, Denilson Mendes de Oliveira, and Andres Urbina for their scientific discussions and support.

Finally, I would like to acknowledge the National Science Foundation for funding the research presented in this dissertation.

TABLE OF CONTENTS

LIST OF TABLES

LIST OF FIGURES

ABBREVIATIONS AND SYMBOLS

A	Area
2BA	2-butyl alcohol
BE	2-butoxyethanol
°C	Celsius
[c]	concentration
CCD	Charge-coupled device
CN	coordination number
d-MeOH	Deuterated methanol
f	Solute interaction fraction
f_{vol}	volume fraction
ΔG	Gibbs free energy
ΔG_B	Gibbs free energy in the bulk
ΔG_S	Gibbs free energy in the hydration shell of the solute
g(r)	radial distribution
H	liquid-like structure
ΔH	enthalpy
ΔH_B	enthalpy in the bulk
ΔH_s	enthalpy in the hydration shell of the solute
H_2O_2	hydrogen peroxide
H_{H2O2}	hydrogen of hydrogen peroxide
H_{water}	hydrogen of water
I	Spectral Intensity
K	equilibrium constant
L	ice-like structure
LiOH	lithium hydroxide
M	molarity
MD	molecular dynamics
n	number of relevant bonds/groups
NaCl	sodium chloride
NaI	sodium iodide
NaOH	sodium hydroxide
O_{H2O2}	oxygen of hydrogen peroxide
O_{water}	oxygen of water
P	Pressure
q	tetrahedral order parameter
R	ratio of Raman cross section
R	gas constant
Raman-MCR	Raman multivariate curve resolution
ΔS	entropy
ΔS_B	entropy in the bulk
ΔS_s	entropy in the hydration shell of the solute

SASA	solvent accessible surface area
SC	solute-correlated
SFG	Sum frequency generation
SHG	second harmonic generation
SMCR	Self-modeling-curve-resolution
T	temperature
T^*	crossover temperature
T_0^*	crossover temperature at infinite dilution
TBA	tert-butyl alcohol
THz	terahertz
TLS	total least squares
$\bar{v}$	partial molar volume
ω	vibrational frequency

ABSTRACT

Open questions remain on the influence of various conditions and ion behavior on the hydration-shell of oily molecules. My research uses Raman spectroscopy and Raman multivariate curve resolution to study the hydration-shell of oily molecules as tools to help answer some of these open questions.

More specifically, I present results on the effect of molecular crowding on the structure of water around various oily molecules, and report the effect of molecular crowding on hydrophobic crossover. These results are important, as crowding has the potential to influence several fields, such as biology and environmental sciences. This work shows that increasing molecular concentration results in oil-oil crowding, decreases the tetrahedrality of the water structure around the oily molecules, and subsequently, the crossover temperature.

In addition to studying the hydration-shell under crowded conditions, I also present work on ion affiliation for the hydration-shell of an oily molecule. Ion affiliation for oil/water interfaces has been an ongoing topic of research since the Hoffmeister experiments because of their effect on biological processes. This study focuses on hydroxide and its affiliation for tert-butyl alcohol in comparison to other electrolytes. These results show iodide is less repelled by the oil/water interface in comparison to hydroxide.

Finally, I present findings on the influence of hydrogen peroxide in comparison to other small molecules on the water structure of an oily molecule. Hydrogen peroxide has been shown to reach supercooled temperatures, which may be useful in future studies of liquid phase transitions or studies on solute behavior at supercooled conditions. It is found that hydrogen peroxide does not significantly influence the water structure around tert-butyl alcohol, while other small molecules display significant water structure changes.

All these projects aim to contribute results to heated debates, as well as share information for future experiments.

CHAPTER 1. RAMAN SPECTROSCOPY, RAMAN INSTRUMENT AND ANALYSIS METHOD

1.1 Raman Spectroscopy background

Raman spectroscopy was used in the following projects to study the molecular behavior of hydrophobic interactions in aqueous media. To collect Raman spectra, a Raman Spectroscopy instrument directs light of a specific wavelength onto a sample. The sample will then absorb or scatter the photons. The photons which scatter will do so elastically or inelastically. The elastically scattered photons have the same frequency as the incident photons (referred to as Rayleigh scattering). The inelastically scattered photons are those which change in frequency from the incident photon.

These inelastically scattered photons fall into one of two categories: anti-Stokes and Stokes scattering. In anti-Stokes scattering, the molecule is in an excited state and will emit energy, then fall to a lower energy level. In other words, the scattered photon has a higher frequency than the incident photon. Stokes scattering, on the other hand, occurs when the molecule is in the ground state and absorbs energy, placing it in a higher energy level. This occurs when the scattered photon has a lower frequency than the incident photon. During this process, Stokes scattering is more prevalent than anti-Stokes scattering, resulting in higher intensity Stokes scattering spectra. The Raman spectroscopy instrument used in the following projects collects Stokes scattering photons and the resulting Raman spectrum.

1.2 Raman Instrument

A home-built Raman system was used to collect all Raman spectra. A 514.45 nm Ar-ion laser (~20mW power) was directed with multiple mirrors and a notch filter through a microscopic lens onto the sample.[1-2] The samples were held in a temperature-controlled cell holder from Quantum Northwest.[3] A Raman 180° photon scatter signal was then collected back through the beam path. Once the back-scattered photons reached the notch filter, the notch filter blocked the incident laser frequency, allowing all other frequencies to pass through more filters and lenses to be focused into the fiber optic cable, which led to the spectrograph and charge-coupled device (CCD) camera. The spectrograph (SpectraPro300i, Acton Research Inc.) has a 300 mm^{-1} focal

length and a grating of 300 grooves per mm^{-1}, with a dispersion of ~ 6 cm^{-1} per CCD pixel, in addition to a thermo-electrically cooled CCD (Princeton Instruments Inc. Pixis 400B, 1,340 X 400 pixel). Between the notch filter and the fiber optic cable, a beam-splitter can be moved into and out of the path to collect polarized spectra. Unless specifically stated, the following spectra are unpolarized.

A neon lamp was used for wavelength calibration, while a helium lamp was used to correct frequency shifts due to environmental changes, such as barometric pressure. Before spectra were collected, a neon lamp was placed in front of the objective and a neon spectrum collected. Six peaks from this neon spectrum were fit to the corresponding CCD pixel positions and converted into wavenumbers. After the neon spectrum was collected, the neon lamp was removed and the samples placed into the cell holder. The helium lamp used for frequency shift corrections was located directly behind the sample and switched on for every sample collection. The helium peaks (Figure 1.1) within each spectrum were used to align the frequency axis across spectra collected on the same day.

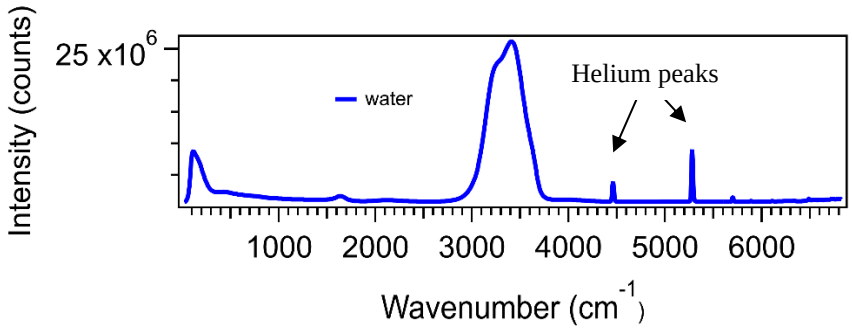

Figure 1.1 Raman Spectra of water with helium peaks used to correct frequencies across spectra.

For example, two spectra collected on the same day would have helium peaks which would then be corrected by overlapping the peaks and shifting the frequency axis to ensure the peaks corresponded to the same frequency. These shifts are less than a pixel, but were corrected because even subtle shifts using the following analysis method could result in spectral artifacts for samples at low concentrations.[1]

1.3 Analysis Methods

1.3.1 Self-Modeling Curve Resolution

Igor-pro software was used to run self-modeling-curve-resolution (SMCR) to obtain Raman multivariate curve resolution (Raman-MCR) spectra. Once a Raman spectrum of a sample was collected, SMCR was used to decompose that spectrum into its correlated spectra to analyze a solute's hydration-shell. This process began with the original spectrum (Figure. 1.2 (A)-(B)), which will be referred to as the raw spectrum, collected from the Raman instrument described in section 1.2. The raw spectrum was shifted to the corrected frequencies determined by the helium peaks described in section 1.2, and smoothed using Savitsky-Golay smoothing. During this shift and smooth step, the background was removed by subtracting the global minimum from the spectrum. After the spectrum was shifted and smoothed, the SMCR analysis was run. SMCR decomposes the raw spectra into correlated spectra by subtracting the raw solvent spectrum from the raw solution (mixture) spectrum to obtain a solute correlated spectrum (Figure 1.2 (C)).[4]

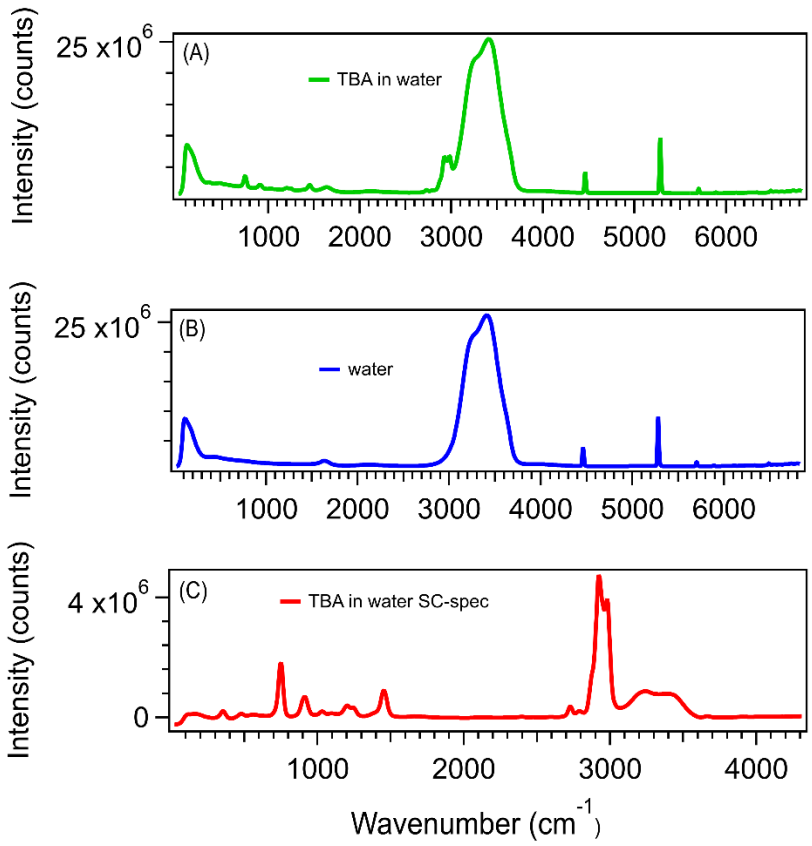

Figure 1.2 Raw Raman spectra of solution and solvent used in Raman SMCR analysis and the resulting SC-spectra (A)-(B) raw solution spectra of TBA in water (0.5M) and water, respectively. (C) The SC-correlated spectra of TBA in water.

This solute-correlated spectrum (SC-spec) contained the vibrational peaks from the solute itself, as well as any solvent molecules perturbed by the solute. In the following chapters, this solvent was typically water. Thereby, the hydration-shell of various solutes was extracted. To better study the water molecules in the hydration-shell, the SC-spec was normalized to specific peaks. For example, the CH stretch region was frequently normalized to better study the changes in the OH stretch region in response to various concentration and environmental changes, depending on the project.

1.3.2 Total-Least Squares and F-Ratio

From the first round of solute-correlated spectra, the three-component mixture SC-spectra were added together using total least squares (TLS) to recreate the vibrational spectra of any perturbed solute by third component ions (Figure 1.3). The TLS method used the solute and co-

solvent SC-spectra, where the solute was typically TBA in water and the co-solvents were a salt (such as NaCl) in water as well as pure water. The three components were then manually adjusted for a non-negative TLS-spectrum residual. In other words, the first round SMCR encompassed the interactions of the solute—water, the salt—water and water—water interactions. TLS then displayed the solute-salt interactions that were not similar to the interactions captured by the first round Raman-MCR spectrum. These interactions were then measured by calculating the fraction of solute-salt interactions to total interactions within the mixture.

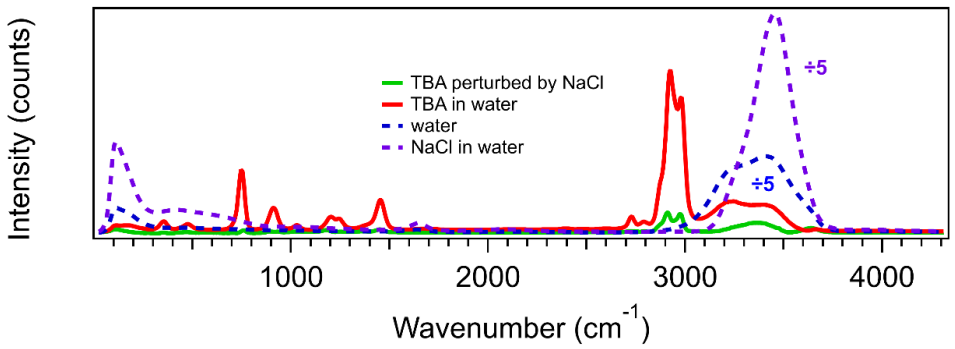

Figure 1.3 TLS-spectra of TBA perturbed by NaCl (solid green) with the three component's SC-spectra TBA in water (solid red), water (dashed blue) and NaCl in water (dashed purple).

CHAPTER 2. INFLUENCE OF CROWDING ON HYDROPHOBIC HYDRATION-SHELL STRUCTURE

Reproduced from A. J. Bredt and D. Ben-Amotz, *Phys. Chem. Chem. Phys.*, 2020, **22**, 11724 **DOI:** 10.1039/D0CP00702A with permission from the PCCP Owner Societies

2.1 Abstract

The influence of molecular crowding on water structure, and the associated crossover behavior, is quantified using Raman multivariate curve resolution (Raman-MCR) hydration-shell vibrational spectroscopy of aqueous tert-butyl alcohol, 2-butyl alcohol and 2-butoxyethanol solutions of variable concentration and temperature. Changes in the hydration-shell OH stretch band shape and mean frequency are used to identify the temperature at which the hydration-shell crosses over from a more ordered to less ordered structure, relative to pure water. The influence of crowding on the crossover is found to depend on solute size and shape in a way that is correlated with the corresponding infinitely dilute hydration-shell structure (and the corresponding first hydration-shell spectra are invariably very similar to pure water). Analysis of the results using a Muller-like two-state equilibrium between more ordered and less ordered hydration-shell structures implies that crossover temperature changes are dictated primarily by enthalpic stabilization of the more ordered hydration-shell structures.

2.2 Introduction

Crowding plays a central role in the self-assembly of biological, polymeric, and environmental systems.[5-8] Numerous prior theoretical [9-15] and experimental[1, 16-26] studies have highlighted the influence of solute size[1, 9-22] and crowding[23-26] on water structure and dynamics, as well as the associated water structural crossover,[1, 9-21] but have not directly probed the influence of crowding on the crossover. Here we do so by measuring the hydration-shell vibrational spectra of aqueous solutions containing the three solutes shown in Fig. 2.1, using Raman multivariate curve resolution (Raman-MCR) spectroscopy.[27] Our results reveal that crowding decreases hydration-shell tetrahedrality and lowers the associated crossover temperature. However, we also find that the hydration-shells of these oily solutes are remarkably similar in structure to bulk water,

even when the solution is sufficiently crowded that there is not enough water to fully populate the solute hydration-shell.

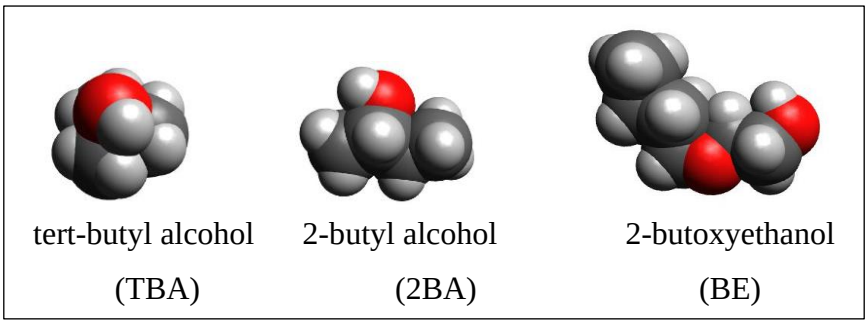

Figure 2.1 Molecular structures of the three solutes

Early theoretical crossover predictions pertained to water containing idealized hydrophobic (hard-sphere) solutes,[9-10] and predicted a dramatic "dewetting" ("drying") crossover from a liquid-like to a vapor-like hydration-shell structure for hard-sphere solutes larger than ~1 nm, although subsequent theoretical studies predicted the suppression of dewetting and aggregation by solute-water attractive interactions.[11, 28-29] Experimental NMR,[16] single-molecule pulling,[17-18] Raman-MCR,[1, 19-21] and THz[22] studies of aqueous solutions containing oily molecular and polymeric solutes confirmed the presence of a crossover length-scale near 1 nm at ambient temperatures, as well as a decrease in the crossover length-scale with increasing temperature (although the experimentally inferred changes in hydration-shell structure are less dramatic than a dewetting transition). The influence of crowding on water structure has previously been investigated using neutron-scattering measurements of concentrated alcohol-water mixtures.[23-26] The results, obtained with the aid of empirical potential structure refinement simulations, imply that water clusters non-randomly in highly crowded solutions, forming pools of nanometer size whose tetrahedral structure is similar to bulk water (while the alcohol molecules in these crowded solutions were found to cluster nearly randomly).[23] The present Raman-MCR results confirm the relative insensitivity of water structure to crowding, but also indicate that crowding tends to disrupt water structure, thus decreasing hydration-shell tetrahedrality and the associated crossover temperature.

Raman-MCR spectroscopy is uniquely suited to quantifying crossover phenomena, as the resulting spectra are exquisitely sensitive to small differences between the structure of pure water

and the hydration-shell of a solute molecule. Prior Raman-MCR studies have quantified the influence of aggregation on hydration-shell structure,[21, 27, 30-32] but have not addressed the influence of crowding on hydrophobic crossover phenomena. The oily solutes shown in Fig. 2.1 were selected in part because of their relatively high aqueous solubility, which is required in order to establish the influence of crowding on hydration-shell structure. Note that a crowded solution is here defined as one in which there is not a sufficient amount of water to fully hydrate all the solute molecules. The results are analyzed using a Muller-like two-state model[33] and compared with previously published results to quantify the influence of solute size and shape on hydration-shell water structure and crossover phenomena.

2.3 Methods

Tert-butyl alcohol (TBA), 2BA and 2-butoxyethanol obtained from Sigma-Aldrich were weighed and diluted to a variety of concentrations with water from a Millipore purification system (H_2O, 18.2 MΩ·cm from Milli-Q UF plus) in 10 ml volumetric flasks. After mixing, each sample was pipetted into a 1 cm glass cuvette and capped. All samples were freshly prepared and used within 24 hrs.

Raman spectra were obtained with a custom-built Raman system as previously described[3] using an Ar-ion excitation laser (514.5 nm, ~20mW power at the sample), a 300 mm focal length spectrograph (SpectraPro300i, Acton Research Inc.), a grating of 300 grooves per mm and a TE cooled CCD camera (Princeton Instruments Inc. Pixis 400B). The samples were temperature controlled to a stability of better than ±0.1°C over a temperature range of 20°C to 100°C using a TE cooled cell holder (Quantum Northwest).[2]

Raman-MCR spectra were obtained using self-modeling-curve-resolution (SMCR)[34] to decompose the measured solution spectra into pure solvent and minimum area solute-correlated (SC) components. The minimum area (non-negative) SC spectra were obtained relative to the local linear baseline of the SC spectra. First hydration-shell spectra were reconstructed from the pure water and background-subtracted SC spectra using hydration-shell coordination numbers (CN) obtained from MD simulation, as previously described (and further explained above and in the SI).[19-20]

The first hydration-shell spectrum was obtained by adding a scaled version of the pure water component to the SC spectrum such that the ratio of the resulting OH band area (integrated

from 3200 cm^{-1} to 3800 cm^{-1}) divided by the CH band in the SC spectrum (integrated from 2795 cm^{-1} to 3045 cm^{-1}) is equal to R*CN*2/nCH, where R is the ratio of the Raman cross sections of water per OH divided by that of the solute per CH. The latter ratio was estimated from experimental measurements of CH areas of solutions of various alcohols of known concentration, divided by the OH area of pure water (scaled by the corresponding concentrations OH and CH groups in the two liquids). Concentration dependent measurements of the CH/OH areas of aqueous solutions indicate that the three solutes have R values of 1.22 for TBA, 1.32 for 2BA, and 1.27 for BE, and it is these values that were used to reconstruct hydration-shell spectra whose area matched the MD simulation prediction of the hydration-shell coordination numbers.

2.4 Results and Discussion

The following is a detailed description of our experimental aqueous 2BA results, followed by a summary of the corresponding results for aqueous TBA and BE (with additional details provided in the SI). As will become evident, each of the three solutes are found to have different hydration-shell structures and crossover temperatures, both at infinite dilution and under crowded conditions, although the hydration-shell structures invariably remain quite similar to liquid water.

Figure 2.2 compares the measured Raman spectra and Raman-MCR spectral components obtained from an aqueous 2BA solution of 0.5 M concentration at 20°C. The dashed blue and dotted purple curves are the measured Raman spectra of pure water and aqueous 2BA. The solid purple curve is the Raman-MCR minimum area solute-correlated (SC) spectrum of 2BA, which contains features arising from the intramolecular vibrations of the solute (including the prominent CH stretch band near 2900 cm^{-1}) as well from hydration-shell water molecules that are perturbed by 2BA (as primarily evidenced in the OH stretch band between 3100 cm^{-1} and 3700 cm^{-1}). Note that previous studies have demonstrated that such SC OH bands arise primarily from perturbed water molecules, rather than the OH head group of the alcohol (due primarily to the far greater number of water OH groups in the hydration-shell).[1, 35] The SC OH band highlights solute-induced perturbations in the OH stretch band of water, as more clearly seen in the inset panel in Fig. 2, which reveals that the SC OH spectrum also contains a small high frequency OH peak near 3660 cm^{-1} resulting from an increased population of non-hydrogen bonded (dangling) OH groups in the hydration-shell.[35-36] Moreover, the lower frequency hydrogen-bonded region of the SC OH stretch band has a different shape than the OH band of pure water, with a lower (red-shifted) average OH

frequency and a more prominent shoulder near 3200 cm^{-1}, both of which indicate that the hydration-shell has a more tetrahedral structure than pure water at this temperature.[1, 19]

The dot-dashed purple curve in Fig. 2 shows the reconstructed spectrum arising from the full first hydration-shell of 2BA. This first hydration-shell spectrum was obtained from a linear combination of pure water and SC spectra, constructed using an MD simulation-based estimate of the number of water molecules in the first hydration-shell (obtained as previously described, and further detailed in the SI).[19-20] More specifically, the MD results indicate that there are ~28 water molecules in the first hydration-shell of 2BA at 0.5M and 20°C (see SI Figure 2.13 and Table 2.2). Since a 0.5 M aqueous solution contains a total of approximately 100 water molecules per solute, the MD results imply that nearly 1/3 of all the water molecules in the solution reside in the 2BA's first hydration-shell at this concentration. More specifically, the reconstructed first hydration-shell spectrum is obtained assuming that the average Raman cross section of water molecules in the first hydration-shell is the same as that in bulk water,[27] and the hydration-shell spectrum is reconstructed from a linear combination of the SC and pure water spectra so as to produce a hydration-shell spectrum whose OH band has an area consistent with first hydration-shell coordination number obtained from the MD simulations.

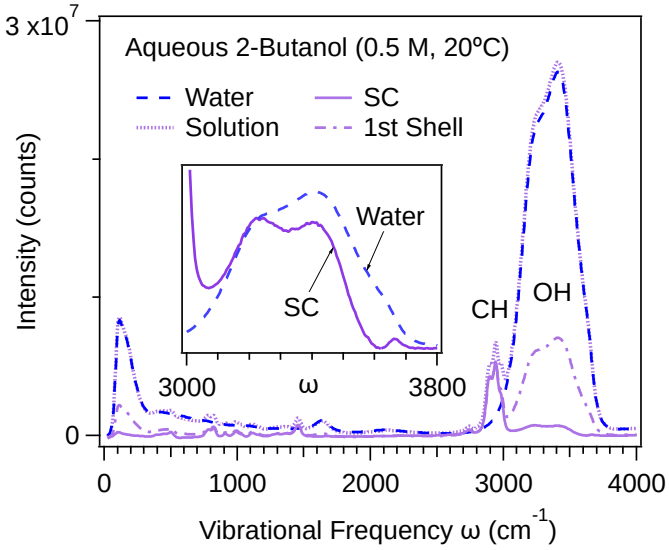

Figure 2.2 Raman spectra of pure water (dashed blue curve) and a 0.5 M aqueous solution of 2BA (dotted purple curve) are compared with the resulting Raman-MCR SC (solid purple curve) and reconstructed first hydration-shell (dot-dash purple curve) spectra. The inset panel compares an expanded view of the OH stretch bands of pure water and the SC spectrum of 2BA (arbitrarily scaled to highlight the differences between the shapes pure water and SC OH stretch bands).

Figure 2.3 shows how varying the temperature and concentration of the solution influence the SC and first hydration-shell spectra of 2BA. The temperature dependence of the SC spectra in solutions of 0.5 M and 2 M concentration are shown in Fig. 3(A) and (B), respectively, with expanded views in the inset panels. Note that all these SC spectra are normalized to the CH band area, and thus the decrease in the SC OH band area with increasing temperature implies that the hydration-shell structure differs most from pure water at low temperatures, and becomes most similar to pure water near 80°C.

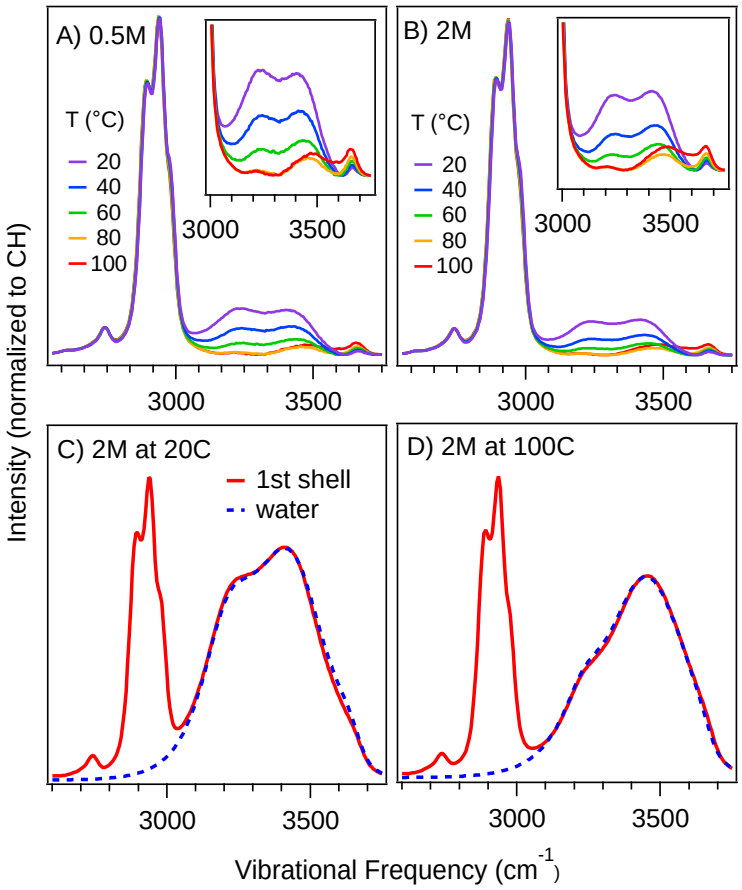

Figure 2.3 The influence of temperature and concentration on the Raman-MCR SC spectra of aqueous 2BA, in the solute CH and hydration-shell OH band regions. (A) and (B) compare the temperature dependence of the SC spectra at solute concentrations of 0.5M and 2M. All the SC spectra are normalized to the CH band area, and thus represent the average SC spectra of a single solute. The inset panel of (A) and (B) contain an expanded view of the SC hydration-shell (OH band) spectra, all plotted on the same scale. Panels (C) and (D) compare the OH stretch region of the full first hydration shell of 2M 2BA (solid red) with bulk water (dashed blue) at 20°C and 100°C, scaled to the OH band peak height in order to highlight the very similar, but slightly shifted, shapes of the hydration-shell and pure water OH bands.

Comparison of the SC OH band areas shown panels Fig. 3(A) and (B) further indicates that at high concentration there are fewer perturbed water molecules in the hydration-shell of each solute – as evidenced, for example, by the difference between the areas of the 20°C (purple) SC OH bands in (A) and (B). This decrease is consistent with the crowding-induced expulsion of water molecules from the solute's hydration-shell, as previously observed in other aqueous solutions.[30-32] Moreover, the change in shape of the SC OH band reveals that crowding leads to a decrease in the relative intensity of the hydration-shell 3200 cm^{-1} shoulder, which implies a decrease in water

tetrahedrality.[1] It is also noteworthy that upon crowding the dangling OH peak frequency increases towards the ~3680 cm^{-1} frequency of dangling OH groups at a macroscopic air-water interface.[37] For example, at 20°C the dangling OH frequency in the hydration-shell of TBA increases from ~3664 cm^{-1} at 1 M to ~3674 cm^{-1} at 4 M (corresponding to a solute volume fraction ~0.35), while that of BE increases from ~3668 cm^{-1} at 1 M to ~3676 cm^{-1} at 3 M (corresponding to a solute volume fraction ~0.36). This suggests that under crowded conditions, the water dangling OH groups exist in a lower local density environment than that in the hydration-shells of a dilute oily solutes.[38]

Figures 2.3(C) and (D) compare the OH band of pure water with the full first hydration-shell spectrum of 2BA at a concentration of 2M and either 20°C (C) and 100°C (D), obtained as described above (with further details in the *Experimental and Data Analysis Methods* section, and the SI).[19-20] The striking similarity of the pure water (dashed blue) and first hydration-shell (solid red) OH bands implies that the structure of water in the first hydration-shell is extremely similar to that of pure water. However, close inspection of the hydration-shell and pure water OH bands reveals that at 20°C the hydration-shell OH band is slightly red-shifted (lower in frequency) than pure water, while at 100°C the hydration-shell is slightly blue-shifted (higher in frequency) than pure water. These very subtle frequency shifts can be quantified by obtaining the average OH frequency, as follows, where ω is the OH vibrational frequency the $I(\omega)$ is the OH band shape (normalized to unit area between ω_1= 3200 cm^{-1} to ω_2 = 3800 cm^{-1}).

$$\langle\omega\rangle = \int_{\omega_1}^{\omega_2} \omega I(\omega) d\omega \qquad (1)$$

The resulting average OH frequencies shifts $\Delta\omega = \langle\omega\rangle - \langle\omega\rangle_0$, where $\langle\omega\rangle_0$ is the average OH frequency of pure water, are plotted in Fig. 4 as a function of both temperature and solute concentration.

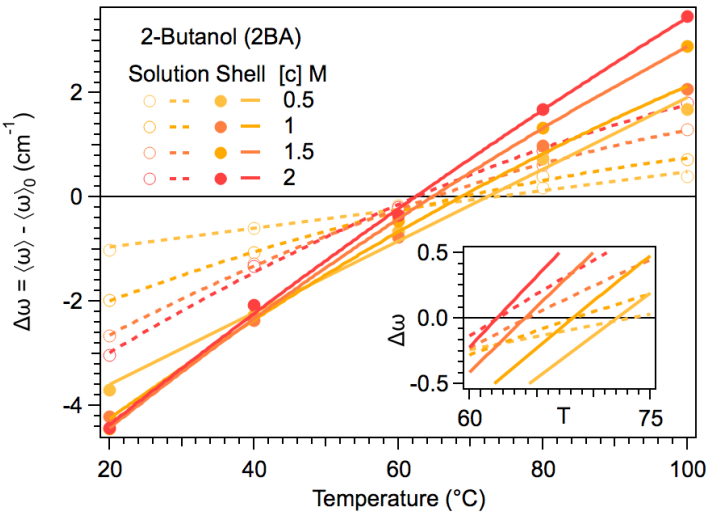

Figure 2.4 Hydration-shell structural crossover is quantified by comparing the average OH frequency in the hydration-shell with that of pure water as a function of solute concentration. The crossover may be obtained either from the OH bands of the Raman-MCR reconstructed first hydration-shells (solid points and lines), or from the OH bands of the measured solution and water spectra (open points and dashed lines). Both procedures yield similar crossover temperatures that decrease with increasing solute concentration, as is more clearly evident in the inset panel showing an expanded view of the crossover region.

The solid curves in Fig. 2.4 correspond to first hydration-shell frequency shifts, and the colors of the curves darken with increasing solute concentration (the significance of the dashed curves is further explained below). The inset panel shows an expanded view of the crossover region, thus more clearly revealing the temperatures at which average OH frequency of the hydration-shell crosses over from negative (red-shift) to positive (blue-shift) values, relative to pure water. These zero-crossing temperatures are those at which the hydration-shell structure most closely resembles that of pure water, and the sign of $\Delta\omega$ (away from the zero-crossing point) indicates whether the hydration-shell is more ordered (negative) or disordered (positive) than pure water. These results reveal that, even over this relatively low concentration range, crowding decreases the crossover temperature by more than 10°C, from a crossover temperature of ~72°C at 0.5 M to ~62°C at 2 M.

The results shown in Fig. 2.4 also demonstrate the insensitivity of the crossover temperatures to the assumed hydration-shell coordination number. This is most clearly illustrated by the dashed lines in Fig. 2.4, which represent the OH frequency shifts obtained directly from the measured solution and pure water OH bands. In other words, the dashed lines are obtained

assuming that all the water molecules in the solution are in the hydration-shell of the solute. The crossover temperatures obtained from the dashed and solid lines are evidently essentially identical (as more clearly seen in the inset panel). However, the frequency shifts (away from the zero-crossing point) decrease with increasing hydration-shell size, as expected, since including more distant water molecules in the hydration-shell increases the spectral similarity of the hydration-shell and pure water. Further implications of the insensitivity of the crossover temperature to hydration-shell size are discussed in the *Conclusions and Implications* Section (as well as in Section 2 of the SI).

At a 2BA concentration of 2M approximately 17% of the system volume is occupied by the solute. Note that the alcohol volume fraction, f_{vol}, is equivalent to the product of its concentration and its partial molar volume ($\bar{v}_{2BA} \approx 0.0866$ M^{-1}, so $f_{vol} = [c]\bar{v}$ = 2x0.0866 ≈ 0.173).[39] Since this concentration is near the solubility limit of 2BA it is not possible to obtain crossover results at higher concentrations. However, the other two solutes, TBA and BE, are infinitely miscible in water (near ambient temperatures). Our crossover results obtained for those solutes extend up to solute volume fractions near 40% (calculated using $\bar{v}_{TBA} \approx 0.0878$ M^{-1} and $\bar{v}_{BE} \approx 0.12$ M^{-1}),[32, 39] and have a correspondingly larger crowding-induced shift in the crossover temperature, as shown in Fig. 2.5. The hydration-shell OH band spectra of these more-crowded solutions still look strikingly similar to the OH bands of pure water (as shown in SI Figs. 2.9-2.11, which also includes crossover results obtained assuming that the hydration-shell coordination number is concentration independent). Note that when fully hydrated the first hydration-shells of the three solutes in Fig. 2.1 contain approximately 30-40 water molecules (see SI Fig. 2.13). This implies that above a concentration of ~1M, or a volume fraction of ~10%, there is no longer enough water to fully hydrate each solute, and thus such solutions are classified as crowded.

Figure 2.5 shows a plot of the crossover temperature, T^*, as a function of volume fraction for the three solutes in Fig. 2.1. The crossover temperatures all decrease upon crowding, but each of the solutes has a different crossover temperature at infinite dilution T_0^* (as obtained from the y-intercepts of the dashed lines in Fig. 2.5) and a different slope with respect to volume fraction. The inset in Fig. 2.5 shows the correlation between the latter crowding-induced slope and the hydration-shell crossover at infinite dilution (along with the dotted best fit line $dT^*/\partial f_{vol} = 2.74T_0^* - 290$). Thus, solutes with higher crossover temperatures at infinite dilution are also less

sensitive to crowding. In other words, hydration-shells that are more ordered at infinite dilution are also less susceptible to crowding-induced disordering.

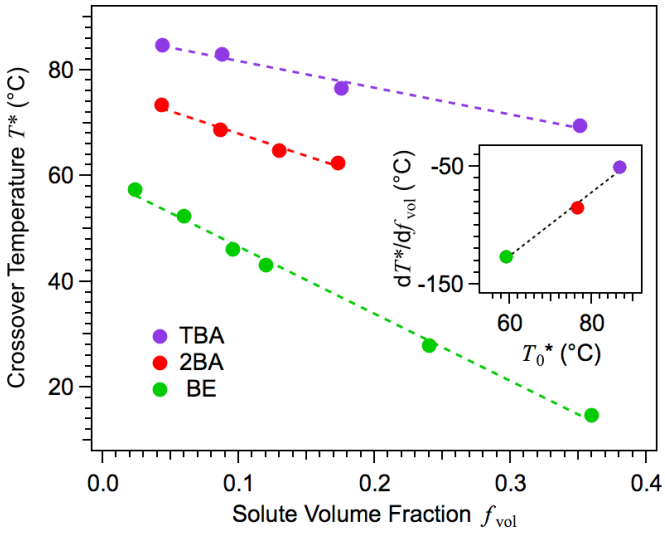

Figure 2.5 The dependence of crossover temperature T^* on solute volume fraction. The y-intercept represents the crossover temperatures at infinite dilution T_0^*. The inset panel shows the correlation between T_0^* and the derivative of T^* with respect to solute volume fraction.

2.5 Conclusion and Implications

Our results reveal that in both dilute and crowded solutions the hydration-shells of oily molecules are more ordered (more tetrahedral) than bulk water below the crossover temperature (T^*), and becomes more disordered above T^*. The associated changes in water tetrahedrality may be quantified by measuring the difference between the average OH frequency in bulk water and the hydration-shell of oily solutes. More specifically, previous experimental and MD simulation studies of pure water have revealed that there is a nearly linear correlation between the average OH frequency and tetrahedrality of water, such that $dq/d\omega \approx$ -0.00173,[19] where q is the Errington−Debenedetti[40] tetrahedral order parameter. Thus, a red-shift of the average OH frequency of water corresponds to an increase in water tetrahedrality (or conversely for a blue-shift). Given that average tetrahedrality of water at 20°C is $q \approx 0.67$, an OH frequency shift of $\Delta\omega$ = 4 cm^{-1} (comparable to the largest shifts shown in Fig. 2.4) corresponds to a tetrahedrality change of ~1%, whose small magnitude is consistent with observed similarity of the pure water and hydration-shell OH bands, as shown in the Fig. 2.3(C) and (D). Note that the correlation between

w and q is only applicable to systems with hydration-shell OH stretch band shapes that closely resemble bulk water, as is the case in the present studies. Moreover, the observed crossover behavior requires that the hydration-shell has a temperature dependent spectral shape, implying the presence of sub-populations of differing temperature dependence, as is evident in both Raman-MCR[1, 19-20] and THz[22] hydration-shell spectra (and further discussed in the SI).

Previous studies have shown that the hydration-shell structural crossover in aqueous n-alcohol solutions is influenced by the length of the alcohol's oily tail, as well as by its OH head group, as the crossover temperature increases from ~60°C for n-butanol to ~160°C for methanol, but decreases to ~80°C for methane.[19-20] This suggests that the crossover temperature is correlated with solutes size, and is increased by the presence of a polar head group. The previously measured crossover temperatures for short-chain n-alcohols (up to n-butanol) are approximately linearly correlated with solvent accessible surface area (SASA), such that T^* increases by 1°C when SASA decreases by ~1 Å^2 (where SASA is obtained assuming a water radius of 1.4 Å). Moreover, comparison of T^* for the three butanol isomers, n-butanol, 2BA and TBA, with 1, 2, and 3 methyl groups, respectively, implies that T^* increases by ~6°C for each solute methyl group. More specifically, a global correlation of the experimental crossover temperatures at infinite dilution for all of the above alcohol solutes (excluding BE) implies that T_0^* (°C) = 314.9 -1.026*SASA + 6.36*nCH_3 (where nCH_3 is the number of methyl groups per solute). This correlation reproduces the experimental crossover temperatures of all these alcohols to within a few degrees (as shown in the SI Table 2.1). However, this correlation does not hold for BE, as its crossover temperature is ~59°C, which is similar to that of n-butanol although BE has a 33% larger SASA of ~336.8 Å^2 (and both solutes have the same number of methyl groups, nCH_3=1). Thus, the ether oxygen in BE evidently has the effect of increasing T^* by ~84°C above that expected for an alcohol of approximately the same size and shape (e.g. n-heptanol). An alternative interpretation of the similar T^* values of BE and n-butanol is that T^* is dictated primarily by the n-butyl chains of these two solutes (and thus that the ethoxy ethyl head group of BE has approximately same influence on T^* as the OH head group of n-butanol).

The formation of perfectly tetrahedral clathrate hydrate solids containing methane and other small oily solutes,[41] implies that clathrate-like structures have a lower (more negative) enthalpy and entropy than liquid-like water structures. In other words, the transformation from a less ordered (liquid-like) to a more ordered (clathrate-like) structure at low temperatures indicates

that clathrate formation is associated with a decrease in both enthalpy ($\Delta H < 0$) and entropy ($\Delta S < 0$). Although, the hydration-shells of oily molecules in liquid water are clearly not solid clathrates, the low temperature hydration-shell spectrum of methane dissolved in liquid water may be accurately represented as a linear combination of pure liquid water and clathrate structures.[20] Moreover, the hydration-shell of methane in liquid water qualitatively resembles the hydration-shells of 2BA, TBA, and BE, and all these oily molecules have hydration-shell structures that are very similar to liquid water.[19-20]

Additional physical insight regarding the influence of crowding on hydration-shell crossover behavior may be obtained by invoking a simple two-state model (in the spirit of the Muller model)[33] to describe the transformation of water from a less ordered to the more ordered structure (as further described in the SI). This analysis suggests that the observation of a crossover temperature requires that ΔH and ΔS in the hydration-shell of an oily solute ($\Delta H_S$and ΔS_S) are not the same as in bulk water (ΔH_B and ΔS_B). Moreover, the observation of a crossover temperature implies that $\Delta H_S < \Delta H_B < 0$ and $\Delta S_S < \Delta S_B < 0$, and $T^* = (\Delta H_S - \Delta H_B)/(\Delta S_S - \Delta S_B)$ (as further explained in the SI). Additionally, this simplified two-state analysis suggests that an increase in T^* results from a greater enthalpic stabilization of the ordered (clathrate-like) water structure, relative to the disordered water structure. Furthermore, the observation that T^* decreases both with increasing solute size and crowding implies that the ordered water structure is enthalpically *destabilized* around large oily solutes and in crowded (oil-rich) solutions. This conclusion is consistent with the observation that increasing either solute size or crowding leads to a breakdown in water tetrahedrality. It is also consistent with the expectation that water near contacting (crowded) oily molecules is disrupted in a way that is qualitatively similar to water around a single larger oily molecule.

In summary, we have quantified the influence of crowding, as well as solute size and shape, on hydration-shell structure, and the associated crossover behavior. However, these results have not addressed the question as to how such water structure changes may influence the water-mediated interactions between oily molecules, including those leading to the self-assembly supramolecular structures such as micelles, vesicles, and bilayers. Theoretical and simulation studies by David Chandler and co-workers have suggested an intimate link between hydrophobic crossover (i.e. drying or dewetting) phenomena and the water-mediated aggregation/collapse of oily molecules.[11] However, it is not yet clear how to reconcile this view with the results of recent

studies[28-29] (and prescient earlier work[42]) pointing to the importance of oil-water attractive (van der Waals) interactions in opposing the aggregation of oily molecules, given that such oil-water van der Waals interactions are expected to be relatively insensitive to water structure. Moreover, recent theoretical,[43] simulation,[44] and experimental[21] studies have reached conflicting conclusions regarding whether the collapse and clouding of oily polymers in water follows[43-44] or precedes[21] dehydration, thus raising further questions regarding the view that hydrophobic collapse is driven by dewetting-related crossover behavior.[43] Additionally, both recent and numerous prior studies[45] indicate that water penetrates deeply into micelles, thus suggesting that the high interfacial tension of macroscopic oil-water interfaces is greatly reduced at molecularly rough non-polar interfaces of micelles composed of either cationic and anionic surfactants. Neutron scattering studies[23-26] have directly addressed the relationship between water structure, crowding, and aggregation in highly concentrated alcohol-water mixtures, and found that water tends to cluster non-randomly in pools of nanometer dimension and highly tetrahedral structure, while the alcohol molecules in these solution are found to have a nearly random structure that is remarkably insensitive to water hydrogen-bonding and clustering.[23] Although these disparate findings remain to be fully reconciled with each other, the emerging picture suggests that the propensity of oily molecules to form crowded aggregates and collapsed structures in water is dictated substantially by competing oil-oil and oil-water van der Waals interactions, rather than by the relatively subtle changes in water structure associated with the crossover phenomena that we have experimentally observed using hydration-shell vibrational spectroscopy.

2.6 Supplementary Information

The following supplementary materials are provided in this document:

2.6.1) A description of the Muller-like model as applied to hydration-shell crossover behavior.

2.6.2) Implications regarding Hydration-shell spectral shape.

2.6.3) Crossover temperature correlation results for alcohol solutes.

2.6.4) Additional Raman-MCR results for TBA, 2BA, and BE.

2.6.5) Additional plots for the three solutes (similar to Fig. 2.4 in the parent manuscript).

2.6.6) MD predictions for the hydration-shell coordination numbers of the three solutes vs. T and [c].

2.6.1 Muller-Like Model of Water Structure

In the spirit of the Muller model,[33] we may describe the structure of water in terms of an equilibrium between structures with (*H*) and (*L*) disorder. In other words, roughly speaking, these two structures correspond to liquid-like (*H*) and clathrate-like or ice-like (*L*) structures (and the former structure is favored at high temperature while the latter is favored at low temperature). The equilibrium between these two structures, $H \leftrightharpoons L$, may be described thermodynamically, as follows.

$$K = \frac{[L]}{[H]} \tag{S1}$$

$$\Delta G = -RT \ln K = \Delta H - T\Delta S \tag{S2}$$

$$\Delta H = \left[\frac{\partial(\Delta G/T)}{\partial(1/T)}\right]_P = RT^2 \left(\frac{\partial \ln K}{\partial T}\right)_P \tag{S3}$$

$$\Delta S = -\left(\frac{\partial \Delta G}{\partial T}\right)_P = \frac{\Delta H - \Delta G}{T} \tag{S4}$$

Note that ΔG and the other thermodynamic state function changes are equivalent to the difference between the corresponding Ben-Naim solvation thermodynamic functions[46] for water in the *L* and *H* structures. Since the population of the more ordered structure decreases with increasing temperature, the temperature derivative of $\ln K$ is negative, and thus $\Delta H < 0$ and $\Delta S < 0$. Note that the latter inequality follows from the fact that the transformation is expressed as that from the more disordered to the more ordered structure. The signs of ΔH and ΔS necessarily hold both in bulk water and in the hydration-shell of an oily solute, but the values of the corresponding enthalpy and entropy changes need not be the same in the bulk (ΔH_B and ΔS_B) as they are in the hydration-shell (ΔH_S and ΔS_S). Moreover, the occurrence of a crossover temperature implies that the temperature derivative of $\ln K$ in the hydration-shell has a larger magnitude than that in the bulk, and thus $\Delta H_S < \Delta H_B < 0$. Furthermore, at the crossover temperature $\Delta G_S(T^*) - \Delta G_B(T^*)$, because at that temperature the equilibrium constant, *K*, is the same in both regions, and thus $\Delta H_S - T^*\Delta S_B = \Delta H_B - T^*\Delta S_B$, which implies that the crossover temperature may be expressed as follows.

$$T^* = \frac{\Delta H_S - \Delta H_B}{\Delta S_S - \Delta S_B} \quad \text{(S5)}$$

Note that since T^* is positive and $\Delta H_S - \Delta H_B$ is negative, that necessarily implies that $\Delta S_S - \Delta S_B$ must also be negative. In other words, the existence of a hydration-shell crossover temperature implies that both the enthalpy and entropy differences between the ordered and disordered water structures are larger (more negative) in the hydration-shell than in bulk water. If it is further assumed that $\Delta S_S - \Delta S_B$ is less sensitive to solutes size and crowding than $\Delta H_S - \Delta H_B$, that would imply that a solute with a larger T^* is one for which the ordered hydration-shell structure is more enthalpically stabilized (has a more negative ΔH_S) than it is for a solute that has a smaller T^*. In other words, this implies that a solute with a higher T^* is one whose shape is such that it can better stabilize a clathrate-like water structure.

The above assumption regarding the relationship between $\Delta S_S - \Delta S_B$ and $\Delta H_S - \Delta H_B$ is consistent with the expectation that the entropy difference between ordered and disordered water structures is dictated primarily by the tetrahedrality of water, rather than by its interaction with the solute, while the enthalpy difference between the ordered and disordered water structures is expected to be strongly influenced by solute-water interactions and thus to be sensitive to solute size, shape, and crowding.

2.6.2 Implications Regarding Hydration-Shell Spectral Shape

Our identification of the crossover temperature as the temperature at which $\Delta\omega$ changes sign relies on the following implicit assumptions and mathematical implications. In order for $\Delta\omega$ to change sign the SC OH band spectrum must have a mean frequency that itself crosses from a lower to a higher frequency than the OH band of pure water as a function of temperature. More specifically, the SC and pure water spectra must be obtained at the same temperatures, the same integration bounds must be used to obtain the average OH frequency. Thus, the observation of $\Delta\omega$ crossover implies that SC spectrum must have a shape that is temperature dependent, and thus may be viewed as consisting of sub-bands of different temperature dependence. These general criteria are satisfied by the SC spectra of the three solutes in Figure 2.1, as well as by the solutes whose hydration-shell spectra have previously been found to undergo a crossover.[1, 19-20, 47] Moreover, our observation that the SC hydration-shell OH stretch bands have a temperature dependent shape is also qualitatively consistent with THz observations that the low frequency

hydration-shell spectra of aqueous alcohol solutions consist of sub-bands of different temperature dependence.[22]

It is also important to note that a crossover in $\Delta\omega$ need not in general imply that the corresponding hydration-shell spectrum (and thus the hydration-shell structure) is similar to that of bulk water. For example, if a SC spectrum consisted of two bands (of arbitrarily large intensity) whose mean frequency was the same as the pure water OH band then the value of $\Delta\omega$ would necessarily be zero but the spectral shape of the hydration-shell might be quite different from that of pure water. Thus, a crossover in the sign of $\Delta\omega$ only implies that the hydration-shell spectrum is similar to water if the intensity of the SC spectrum is also minimized near the crossover temperature, as is the case with all of the SC hydration-shell spectra of interest in this work. In other words, as previously shown[20] the crossover temperature obtained from the temperature at which $\Delta\omega$ crosses zero is also invariably near the temperature at which the SC spectrum has a minimum area. Note that the fact that the SC spectra have an area that is minimized near the crossover temperature is also evident in the spectra shown in Figure 2.3A and 3B of the parent manuscript, as well as Figures 2.6-2.8 below.

Finally, note about the invariance of the crossover temperature to the assumed size of the hydration-shell is consistent with fact that SMCR decomposes the measured spectrum into a linear combination of the pure water and SC spectra. Thus, the temperature at which $\Delta\omega = 0$ is that at which the mean frequency of the SC spectrum is equal to the mean frequency of the corresponding pure water spectrum. This also implies that at the crossover temperature any linear combination of the two pure water and SC spectra must also have the same mean frequency as pure water. Since the assumed number of water molecules in the hydration-shell only changes the relative weights of the pure water and SC spectrum in the total hydration-shell spectrum, the crossover temperature must be independent of the assumed hydration-shell size.

2.6.3 Crossover Temperature Correlation

The following table contains crossover temperatures at infinite dilution for 6 alcohol solutes, as well as the solvent accessible surfaces area (SASA) and number of methyl groups (nCH_3) of each solute. The fit values T_0^* in the last column are predicted using the following expression (fit to the experimental data points): T_0^* (°C) = 314.9 -1.026*SASA + 6.36*nCH_3.

Table 2.1 Crossover temperature correlation for alcohol solutes

Solute	SASA ($Å^2$)	nCH_3	T_0^* (Expt.) (°C)	T_0^* (Fit) (°C)
Methanol	155.6	1	164	162
Ethanol	191.8	1	120	125
1-Propanol	222.3	1	95	93
1-Butanol	252.7	1	62	62.
2BA	246.1	2	76.5	75.2
TBA	240.5	3	86.7	87.2

2.6.4 Additional Raman-MCR Results

The following three Figures contain temperature and concentration dependent SC spectra of TBA, 2BA, and BE.

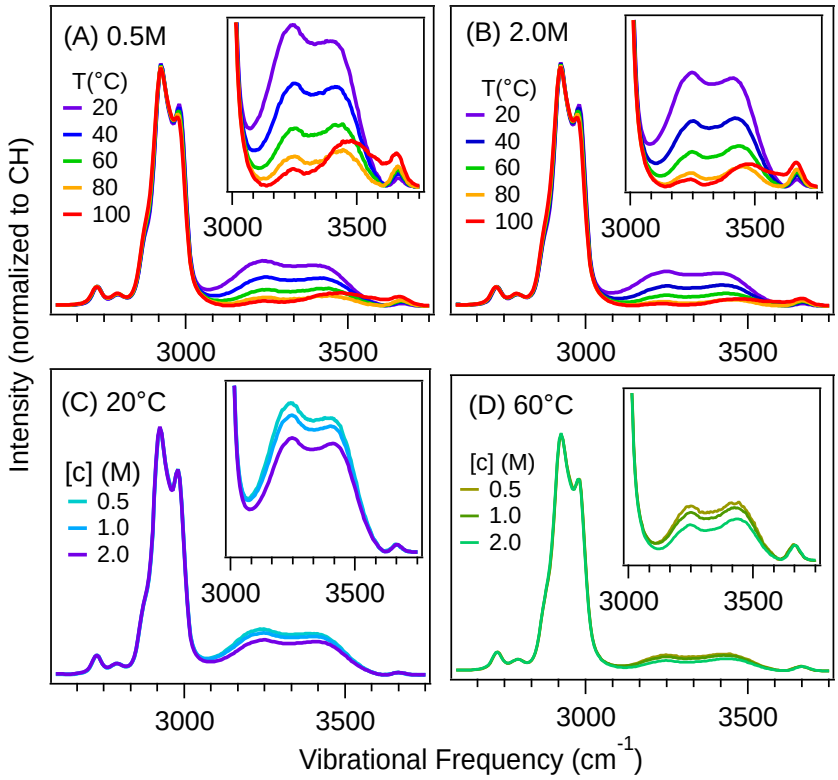

Figure 2.6 The influence of temperature and concentration on the Raman-MCR SC spectra of aqueous tert-butyl alcohol (TBA), in the solute CH and hydration-shell OH band regions. (A) and (B) compare the temperature dependence of the SC spectra at solute concentrations of 0.5M and 2M. (C) and (D) compare the concentration dependence of the SC spectra at 20°C and 60°C. All the spectra are normalized to the CH band area, and thus represent the average SC spectra of a single solute. The inset panel contain an expanded view of the SC hydration-shell (OH band) spectra, all plotted on the same scale.

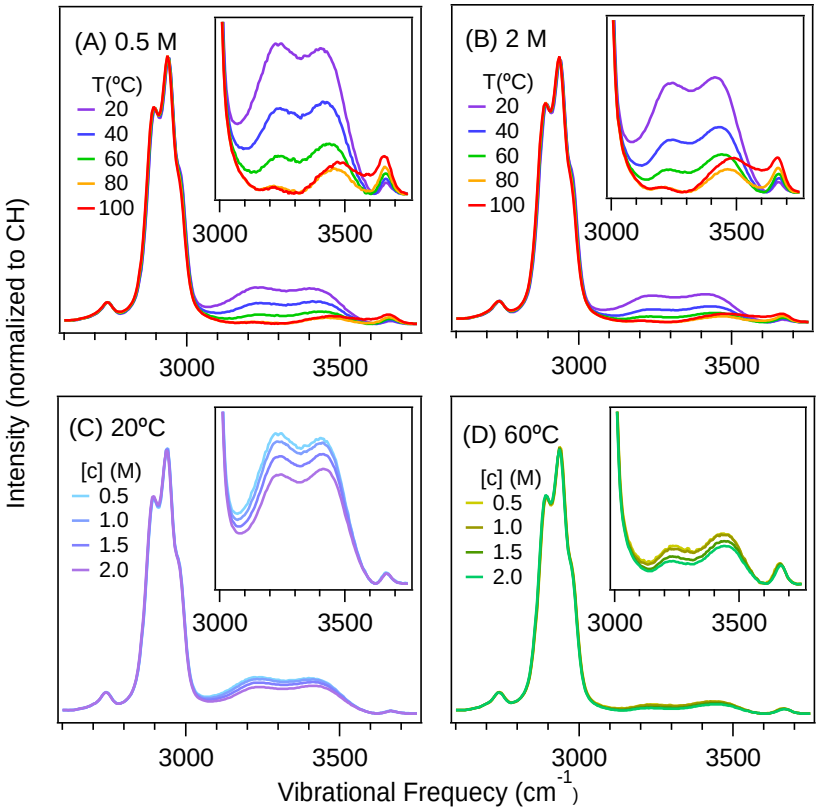

Figure 2.7 The influence of temperature and concentration on the Raman-MCR SC spectra of aqueous 2-Butanol, in the solute CH and hydration-shell OH band regions. (A) and (B) compare the temperature dependence of the SC spectra at solute concentrations of 0.5M and 2M. (C) and (D) compare the concentration dependence of the SC spectra at 20°C and 60°C. All the spectra are normalized to the CH band area, and thus represent the average SC spectra of a single solute. The inset panel contain an expanded view of the SC hydration-shell (OH band) spectra, all plotted on the same scale.

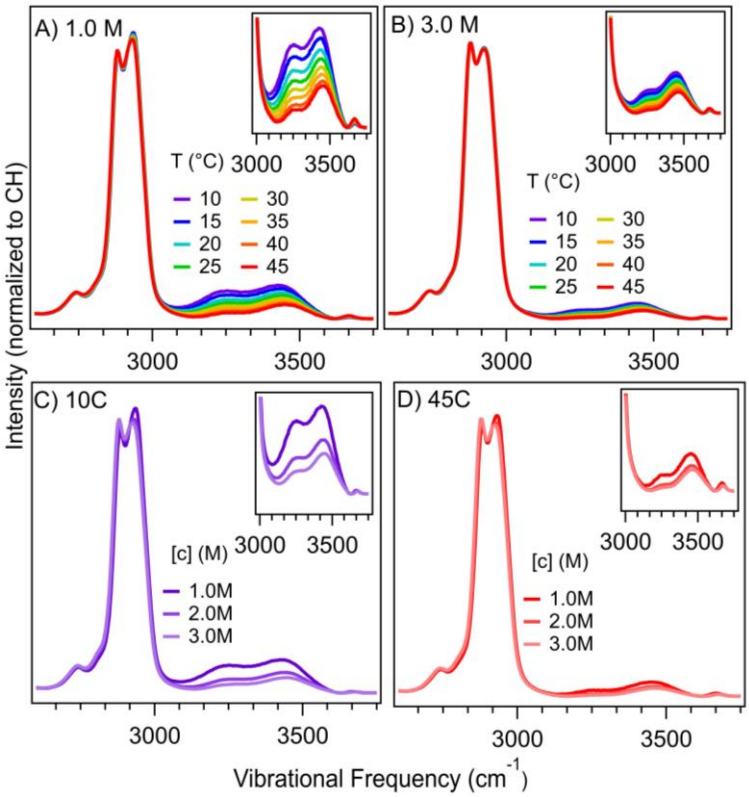

Figure 2.8 The influence of temperature and concentration on the Raman-MCR SC spectra of aqueous 2-butoxyethanol (BE), in the solute CH and hydration-shell OH band regions. (A) and (B) compare the temperature dependence of the SC spectra at solute concentrations of 1M and 3M. (C) and (D) compare the concentration dependence of the SC spectra at 10°C and 45°C. All the spectra are normalized to the CH band area, and thus represent the average SC spectra of a single solute. The inset panel contain an expanded view of the SC hydration-shell (OH band) spectra, all plotted on the same scale.

2.6.5 Additional Crossover Results

The following three figures are similar to Fig. 2.4 in the parent manuscript, except for the addition of the dot-dashed curves obtained assuming that the first hydration-shell coordination number is equal to its predicted value at infinite dilution (ID). The solid curves in Fig. 2.4 and the following three figures are obtained assuming that the first hydration-shell coordination numbers decrease with increasing solute concentration, as predicted using the MD simulations (see Figs. 2.12 and 2.13, and Table 2.2). The dashed curves in Fig. 2.4 and the following three figures assume that all the water molecules in the solution are in the hydration-shell of the solute. The agreement between the crossover temperatures obtained using these three assumptions confirms that the

experimentally derived crossover temperatures are insensitive to the assumed hydration-shell coordination numbers.

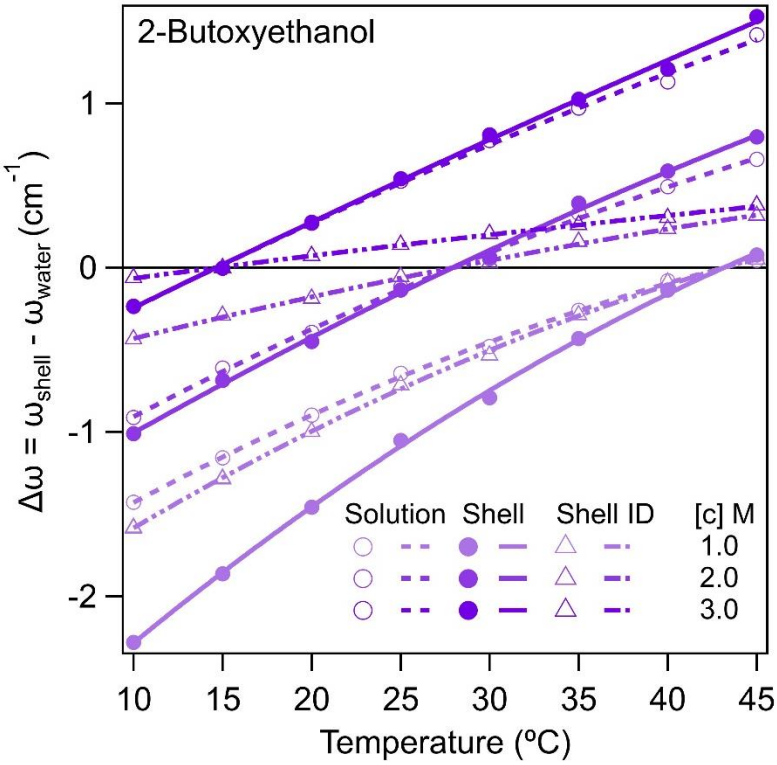

Figure 2.9 Hydration-shell structural crossover is quantified by comparing the average OH frequency in the hydration-shell with that in bulk water as a function of solute concentration. The crossover may be obtained either from the OH bands of the measured solution and water spectra (open circular point and dashed lines) or from the OH bands of the Raman-MCR reconstructed first hydration-shells (solid points and lines) or from the OH bands of the first hydration-shells at infinite dilution (ID, open triangular point and dashed lines). All procedures yield similar crossover temperatures that decrease with increasing solute concentration.

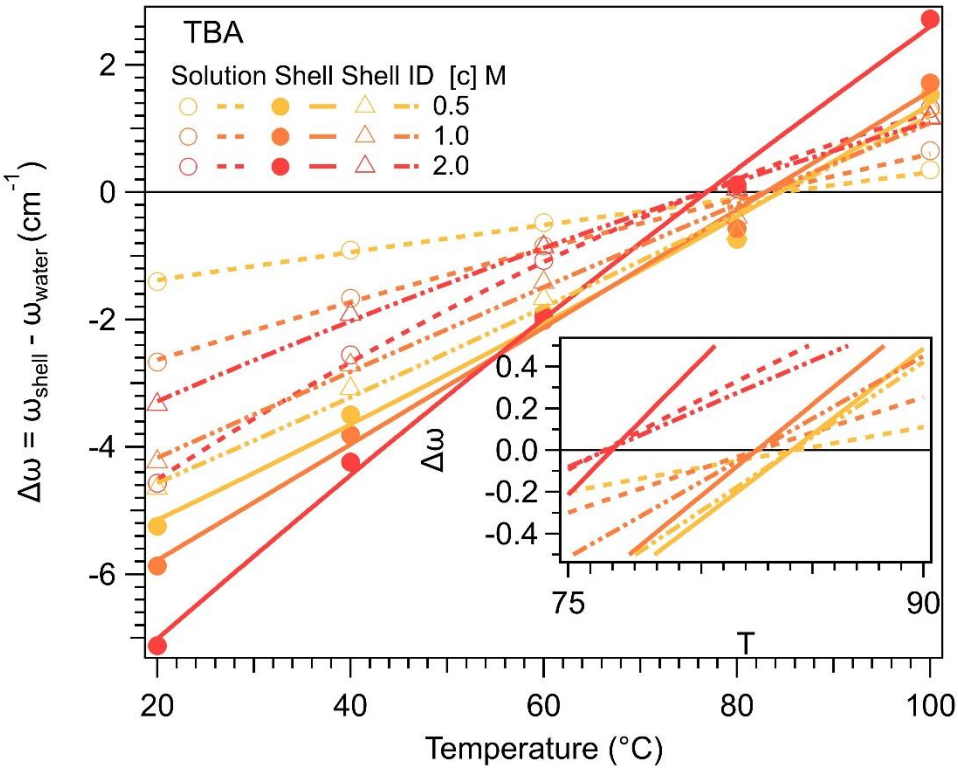

Figure 2.10 Hydration-shell structural crossover is quantified by comparing the average OH frequency in the hydration-shell with that in bulk water as a function of solute concentration. The crossover may be obtained either from the OH bands of the measure solution and water spectra (open circular points and dashed lines) or from the OH bands of the Raman-MCR reconstructed first hydration-shells (solid circular points and lines) or from the OH bands of the first hydration-shells at infinite dilution (ID, open triangular point and dashed lines). All procedures yield similar crossover temperatures that decrease with increasing solute concentration.

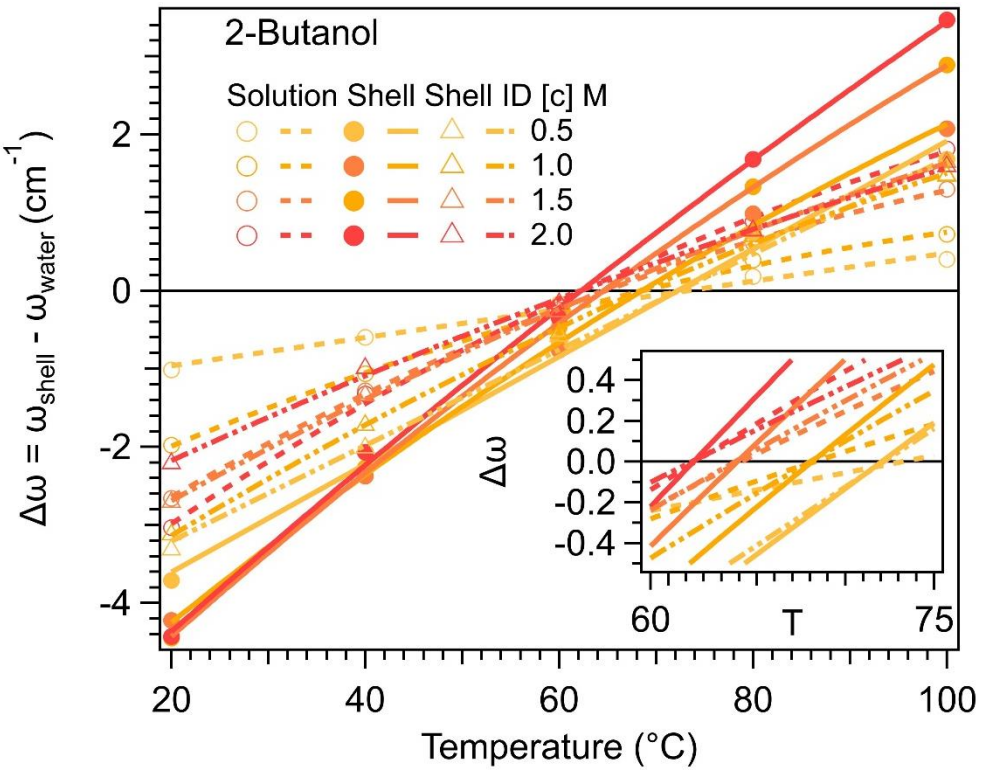

Figure 2.11 Hydration-shell structural crossover is quantified by comparing the average OH frequency in the hydration-shell with that in bulk water as a function of solute concentration. The crossover may be obtained either from the OH bands of the measure solution and water spectra (open circular points and dashed lines) or from the OH bands of the Raman-MCR reconstructed first hydration-shells (solid circular points and lines) or from the OH bands of the first hydration-shells at infinite dilution (ID, open triangular point and dashed lines). All procedures yield similar crossover temperatures that decrease with increasing solute concentration.

2.6.6 MD Coordination Number Predictions

The MD coordination number simulations were performed using GROMACS[48] as previously described,[20] with the following additional details. The solute and water potentials are TraPPE-UA[49] and TIP4P/2005,[50] respectively. The simulations were each run for 100 ns (after 5 ns of pre-equilibration) with 256 water molecules and a variable number of solute molecules, spanning a concentration range between 0.2 M and 4 M. Given the relatively small system size of these simulations (with 256 water molecules), one does not expect the simulations to accurately describe solute aggregation statistics, and particularly the formation of higher-order solute clusters. However, this limitation does not influence our conclusions, as the simulations results are used only to obtain estimates of the hydration-shell coordination numbers, and to show that the resulting

experimentally-derived crossover temperatures are insensitive to the assumed coordination number values.

Figure 2.12 shows representative examples of the radial distribution function for the water oxygen around any solute carbon atom. The water coordination numbers were obtained by integrating the total number of unique water molecules out to a cut-off distance of 0.636 nm from any solute carbon atom (as indicated by the dashed vertical line in Fig. 2.12). The term unique indicates that water molecules that are within the cut-off distance from more than one solute carbon atom are only counted once.

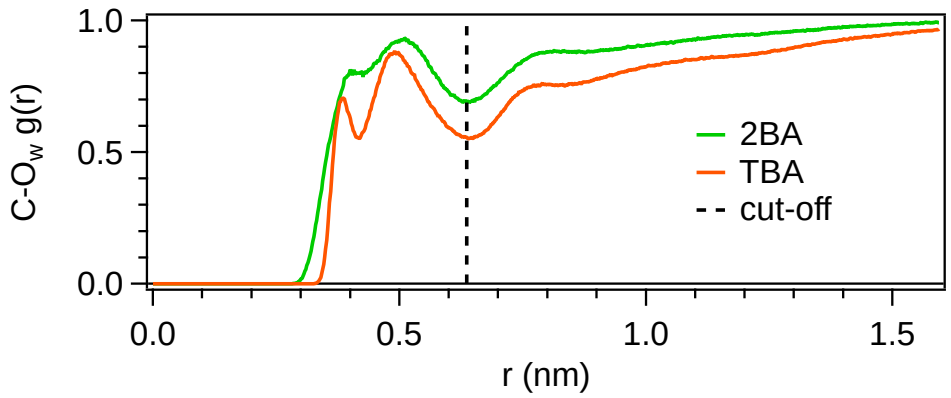

Figure 2.12 Radial distribution functions between solute carbon and water oxygen atoms of 2BA and TBA obtained at 323.15K (50ºC). The vertical dashed line indicates the cut-off value of 0.636 nm that is used to obtain the water coordination numbers surrounding the carbon atoms of all three solutes.

Figure 2.13 shows MD predictions of the hydration-shell coordination numbers for the three solutes as a function of temperature and concentration, obtained as previously described.[20] Table 2.2 contains the polynomial fit coefficients that can be used to re-generate the coordination number predictions. The temperature dependent coefficients, K0-K3 are those used to obtain the coordination numbers (CN) using the bottom equations in Table 2.2. The temperature (T) is in Kelvin units (equal to T ºC+273.15), and the solute concentration (conc) is in M units.

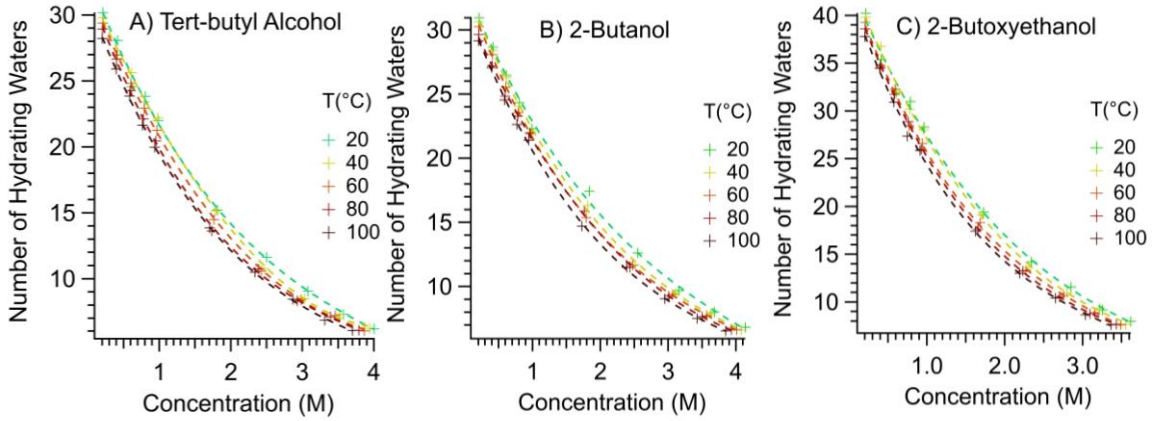

Figure 2.13 The calculated number of waters in the first hydration shell of the solute CH_2 or CH_3 groups obtained from MD simulations of (A) tert-butyl alcohol (TBA), (B) 2-butanol (2BA) and (C) 2-butoxyethanol (BE), as a function of temperature and concentration.

Table 2.2 Polynomial fit to the MD coordination numbers.

A) Tert-butyl Alcohol	B) 2-Butanol	C) 2-Butoxyethanol
$K0=21.325+0.084938*(T)-0.00015666*(T^2)$	$K0=13.461+0.13864*(T)-0.00024012*(T^2)$	$K0=0.10603+0.28822*(T)-0.00047158*(T^2)$
$K1=-16.619+0.040578*(T)-9.3318E-05*(T^2)$	$K1=40.849-0.31209*(T)+0.00044729*(T^2)$	$K1=82.505-0.60592*(T)+0.00087212*(T^2)$
$K2=16.991-0.10182*(T)+0.00017186*(T^2)$	$K2=-15.16+0.0981570*(T)-0.00013698*(T^2)$	$K2=-42.205-0.26817*(T)-0.00037894*(T^2)$
$K3=-3.4604+0.021814*(T)-3.5254E-05*(T^2)$	$K3=1.2094-0.075331*(T)+1.033-05*(T^2)$	$K3=5.7889+0.035231*(T)-4.9524-05*(T^2)$
resulting coordination number equation	resulting coordination number equation	resulting coordination number equation
$CN=K0+K1*(conc)+K2*(conc^2)+K3*(conc^3)$	$CN=K0+K1*(conc)+K2*(conc^2)+K3*(conc^3)$	$CN=K0+K1*(conc)+K2*(conc^2)+K3*(conc^3)$

CHAPTER 3. HYDROXIDE AFFINITY FOR OIL/WATER INTERFACE

3.1 Abstract

Hydroxide's affinity for an oil/water interface is analyzed by Raman-MCR to determine the extent to which hydroxide perturbs an oily molecule, tert-butyl alcohol. Prior experiments have demonstrated sodium iodide is less repelled from the hydration-shell of tert-butyl alcohol, and have shown the extent to which iodide is able to penetrate the hydration-shell. This study is an extension which compares the ion affinity of sodium iodide to sodium hydroxide. To measure this affinity, a total-least squares (TLS) analysis is used to recreate the non-negative residual of the tert-butyl alcohol perturbed by the salt. From this residual, the fraction of perturbed solute is calculated. These results show a higher fraction of iodide-perturbed solutes in comparison to hydroxide-perturbed solutes, thus indicating that iodide is less repelled from the oil/water interface in comparison to hydroxide.

3.2 Introduction

The behavior of ions at molecular interfaces has been of interest since Hofmeister's studies of protein denaturation in various aqueous salt solutions.[51] Hofmeister observed some salts cause proteins to denature, while other salts stabilize the protein. These observations have since been expanded upon by the Debye-Hückel theory. This theory was the first dielectric continuum model to precisely predict experimental results for bulk electrolytes and give a picture of the molecular behavior.[52] Before this theory was proposed, experiments involving surface tension of oil[53-54] and aqueous electrolyte solutions[55] introduced to water were already being reported with little explanation of the interfacial observations. Subsequent theoretical calculations and refinement were completed by Wagner, Onsager and Samaras which better matched experiments at low concentrations; however, these surface tension calculations deviate significantly from experiment at high concentrations.[56-57] In addition, more recent experiments show that some ions are not repelled from the interface, and instead seem to reside at the interface.[58-62] Further theory work by Levin proposed polarizability of ions contribute to this attraction of ions to the interface.[63] However, while simulation and theory have improved to explain experimental observations and

results of halides at the interface, there are still contradictory experimental/simulation results regarding the affinity for these strong electrolytes at the air/water and oil/water interface.

Further study of the attraction or repulsion of strong electrolytes, such as hydroxide, for the oil/water interface is important for several fields such as protein folding, medicine delivery and environmental cleanup.[64-66] Some theoretical studies suggest hydroxide ions remain in the bulk,[67] while other simulations show hydroxide is attracted to the interface.[68-69] There are few experimental studies conducted on hydroxide affinity specifically for the oil/water interface, but some have speculated that any negative charge accumulation at the oil/water interface is due to the accumulation of hydroxide ions at the interface.[58, 70-73] Creux et. al.,[71] go so far as to claim that hydroxide is strongly attracted to both the air/water and oil/water interfaces, more so than a proton or chloride ion. The apparently conflicting simulation and few existing experimental results demonstrate that the interaction between hydroxide and oily molecules is still an open question. Here we present results that contribute to addressing this question by comparing the affinities of iodide and hydroxide for the hydration-shell of an oily solute dissolved in aqueous salt solutions.

In this chapter, molecule behavior is studied by examining both the hydration-shell of tert-butyl alcohol (TBA), as well as the recreated non-negative residual of TBA-perturbed spectra in sodium iodide and sodium hydroxide solutions (I^-, OH^-) with Raman spectroscopy, self-modeling curve resolution (SMCR)[34] and total least squares (TLS). Past studies have shown iodide penetrates the hydration-shell of TBA more than other halides.[74-75] The present results agree with the past literature results on iodide affinity for TBA and expands the results to encompass hydroxide, thereby elucidating hydroxide's place in the attraction/repulsion series of oil molecules.

3.3 Methods

Tert-butyl alcohol (Sigma-Aldrich, ≥99.7%), sodium iodide (Sigma-Aldrich, ≥ 99.5%) and sodium hydroxide (Acros Organics, 98.5%) were used to make three component systems using the following procedure. The three component systems were created by first weighing the salt and the TBA into individual 10 ml volumetric flasks and diluting to 1M and 0.5M, respectively, with water from a Millipore purification system (H_2O, 18.2 MΩ·cm from Milli-Q UF plus). Afterward, TBA was weighed into a 5ml volumetric flask, and the aqueous salt from the previous step used to dilute the TBA to 0.5M. Each volumetric flask was inverted several times to ensure all solids were dissolved, and the solutions were pipetted into glass cuvettes and capped. All glassware was

previously washed and stored in an oven overnight. All samples were freshly prepared, and data taken within 24 hrs.

The samples were collected at 20°C using the Raman system described in section 1.2, and analyzed to obtain the SC-spectra and TLS-spectra using the methods in section 1.3.

3.4 Results and Discussion

The following section will expand on the experimental results of the three component mixtures of TBA, water, and various aqueous ions (NaI, NaOH and LiOH). While the hydration-shell of TBA in the aqueous solutions does not show significant C-H stretch perturbation in comparison to TBA in water, the TLS method manually adds the mixture's components to reveal TBA's which are perturbed by the salt. Further, in this section it will become clear that the degree to which the TBA is perturbed by the salt is dependent upon the type of anion.

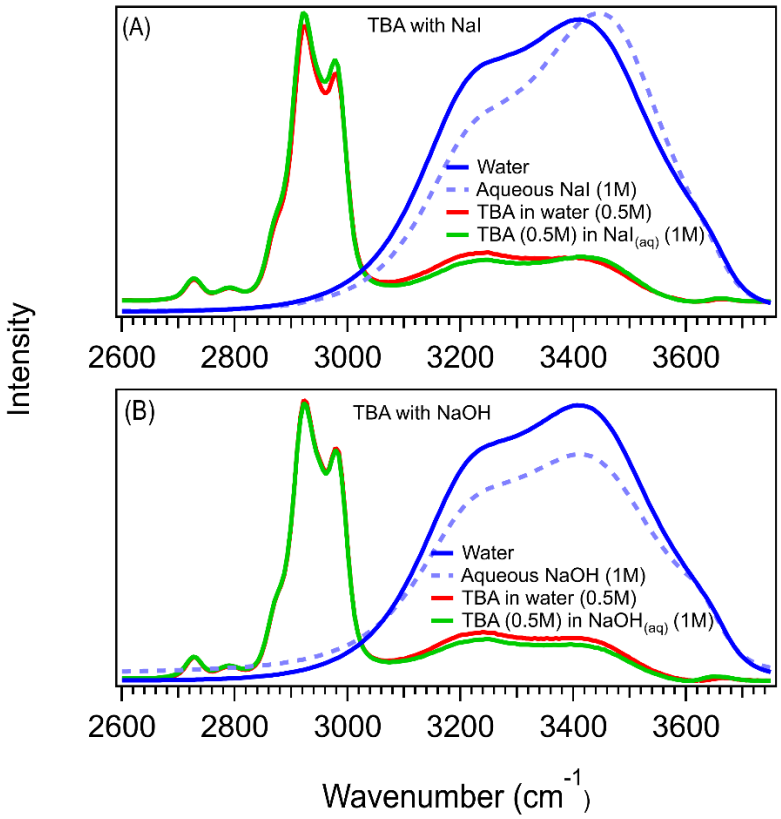

Figure 3.1 Raman-MCR SC-spectra in the solute CH and hydration-shell OH band regions. (A) and (B) compare the SC spectra of TBA (0.5M) in NaI (1M) (solid green trace) versus TBA (0.5M) in NaOH (1M) (solid green trace). Where the solid red trace is TBA in water (0.5M), the solid blue trace is water, and the dashed light-blue trace is the aqueous salt [NaI (1M) and NaOH (1M), respectively]. TBA in NaI data collected by Denilson Mendes de Oliveira.

Figure 3.1 displays the solute correlated spectra of TBA in water, TBA in aqueous salt, aqueous salt, and water. The solid red and green traces are the minimum area solute correlated spectra of TBA and any perturbed solvent, otherwise known as the hydration-shell, which is comprised of the vibrations from the solute and closest perturbed solvent molecules. The solid red trace is the hydration-shell of TBA in water, and the solid green trace is the hydration-shell of TBA in aqueous salt. The O-H stretch from 3100-3800 wavenumbers is a combination of the O-H groups on the TBA and water molecules. The C-H stretch from 2660-3030 wavenumbers, on the other hand, consists only of vibrations from the solute and gives the most information about ions which may penetrate the hydration-shell and perturb the TBA. However, as can be seen, the differences between the C-H stretch of both the red and green traces is insignificant and does not reveal the attraction or repulsion the ions have for TBA. To better uncover the behavior of ions at the oil/water interface of TBA, the spectra have to be further decomposed from TBA perturbed by

aqueous salt into TBAs which are perturbed by the ions. To accomplish this task, TLS was used to find the residual spectral features of the three-component solutions. The TLS method uses the solute, co-solvent and three-component mixture in water SC-spectra to manually obtain a non-negative minimum area residual spectrum, which will be referred to as the TLS-spectrum and is further explained in section 1.3.2. This TLS analysis yields similar results to the ion-correlated spectra obtained with a previously published method[75] where NaI is shown to be less repelled by the oily solute in comparison to NaF, which is significantly repelled. As a result, TLS is used to analyze the data in this chapter.

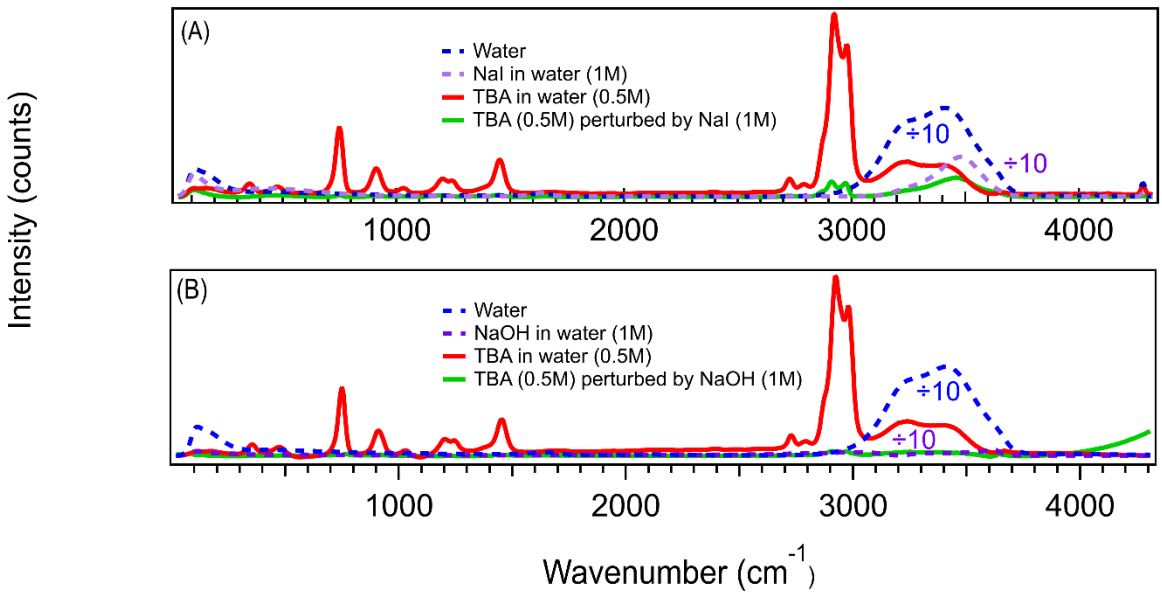

Figure 3.2 Raman-MCR SC spectra of the non-negative TLS-spectrum of TBA (0.5M) by the salts (1M) (solid green), TBA in water (solid red, 0.5M), salt in water (dashed purple, 1M) and water (dashed blue curve). (A) and (B) compare the full SC spectra of TBA perturbed by NaI (A) versus NaOH (B). TBA in NaI data collected by Denilson Mendes de Oliveira.

Figure 3.2 displays the TLS-spectrum along with the solute and co-solvents which are used to obtain the TLS-spectrum. The solid red trace is the solute, TBA in water; the dashed purple trace is the co-solvent salt in water; the dashed blue trace is the other co-solvent, pure water; and the solid green trace is the TLS-spectrum for the salts NaI and NaOH in Figure 3.2 (A) and (B), respectively. When visually comparing the TLS-spectrum of TBA perturbed by NaI [Figure 3.2 (A)] versus TBA perturbed by NaOH [Figure 3.2 (B)], one can see that the intensity of the TLS-spectrum for NaI is larger than that of NaOH, suggesting the number of TBA ions perturbed by

NaI is greater than the number perturbed by NaOH. In fact, the CH stretch seems to be negligible in comparison to NaI, which would suggest that NaOH is repelled by the oil/water interface. However, upon closer inspection and analysis of the CH stretch, there is a small perturbation of TBA by NaOH.

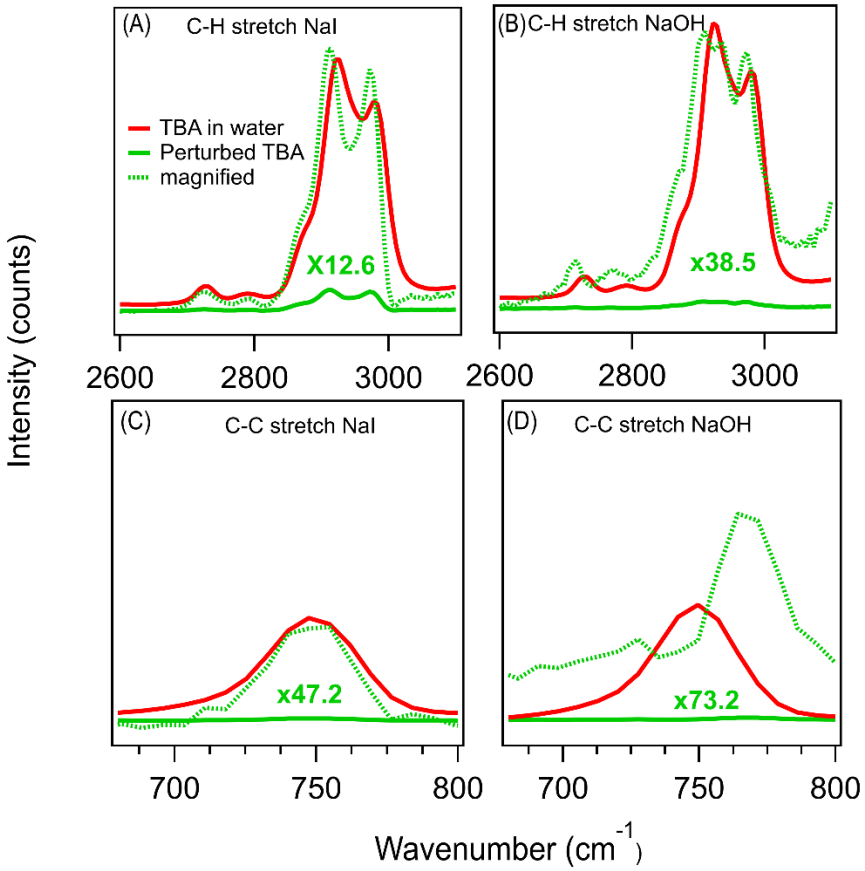

Figure 3.3 C-H and C-C band regions of the Raman-MCR SC spectra of the non-negative TLS-spectrum of TBA (0.5M) by the salts (1M) (solid green) and TBA in water (solid red, 0.5M). (A) and (B) compare the solute CH band region of TBA perturbed by NaI versus NaOH along with the TLS-spectra magnified to the area of the CH stretch of TBA in water (dashed green), while (C) and (D) compare the solute CC band region of TBA perturbed by NaI versus NaOH along with the TLS-spectra magnified to the area of the CC stretch of TBA in water (dashed green). TBA in NaI data collected by Denilson Mendes de Oliveira.

Figure 3.3 focuses on the C-H and C-C stretch for both TBA in water SC-spectrum and TLS-spectrum. The solid green trace is the C-H and C-C stretch of the perturbed TBA, while the solid red trace is that of TBA in water. Again, the solid green C-H stretch TLS-spectrum of perturbed TBA by NaI is larger than that of the solid green trace of TBA perturbed by NaOH. To

quantify the degree of perturbation of the salt on TBA, the fraction of TBA-salt interactions to total molecular interactions is calculated by the following:

$$f = \frac{A_I}{A_T} = \frac{I_{TLS}}{I_{TBA}+I_{TLS}} \quad \text{(I)}$$

Where the f-ratio is the fraction of CH stretch area of perturbed TBA (A_I) divided by the CH stretch area of the total interactions of the CH stretch (A_T), or the intensity of the TLS CH stretch (I_{TLS}) divided by the intensity of the TLS CH stretch and the intensity of the CH stretch of TBA in water (I_{TBA}). This ratio gives a lower bound estimate of the amount of TBA which is perturbed by the salt. In other words, this ratio can be used to estimate the degree to which an ion penetrates the TBA hydration-shell.

The f-ratio for the C-H stretch (2820-3075 cm^{-1}) of NaI is f_{CH}= 7.6%, while the f-ratio of the C-H stretch for NaOH is f_{CH}= 2.6%. This indicates that NaI is less repelled by the oily solute, which agrees with past literature. This also indicates that while NaOH does not seem to perturb TBA, there is a small but measurable amount of perturbation by NaOH. This small perturbation suggests that NaOH is more strongly repelled by the oil/water interface in comparison to NaI, in direct contrast to Creux at al,[71] who claim hydroxide is strongly attracted to the oil/water interface. The solid green C-C stretch of the TLS-spectrum is a much smaller peak in comparison to the C-H stretch for both NaI and NaOH. The f-ratio for the C-C stretch (665-815 cm^{-1}) of NaI is f_{CC}= 2.2%, while the f-ratio of the C-C stretch for NaOH is f_{CC}= 1.3%. The larger C-H f-ratio suggests the salts may linger close to the methyl groups of TBA.

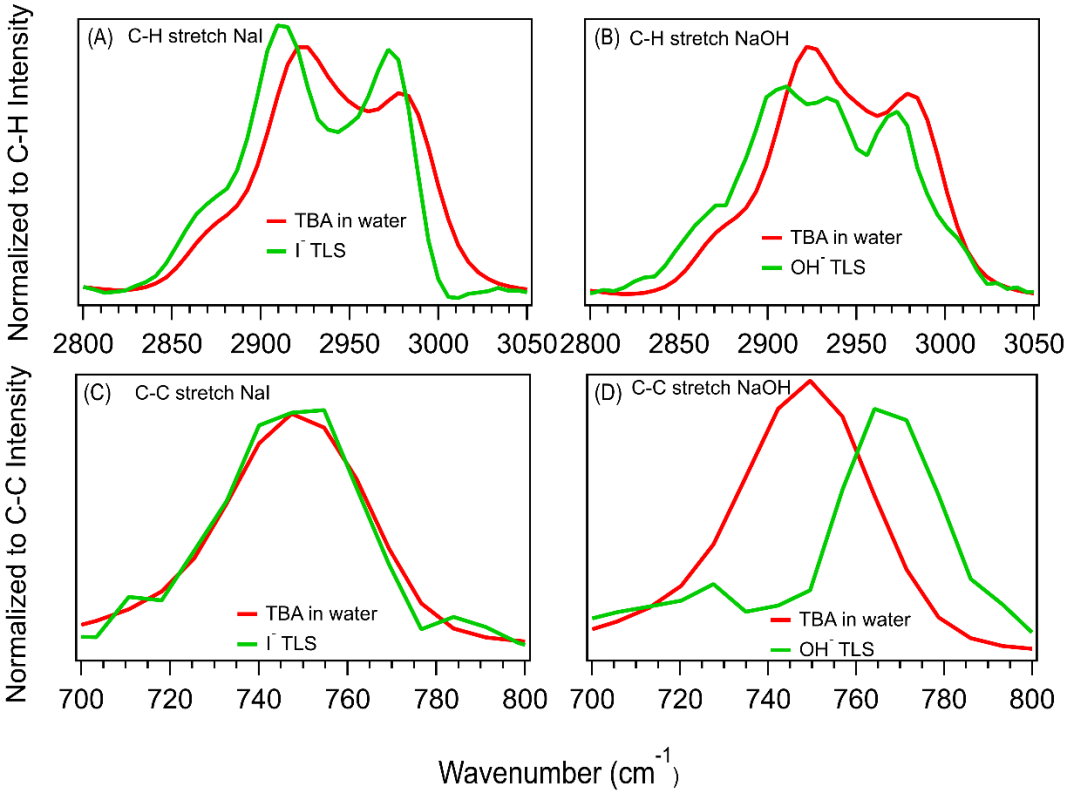

Figure 3.4 C-H and C-C normalized band regions of the Raman-MCR SC spectra of the non-negative TLS-spectrum of TBA (0.5M) by the salts (1M) (solid green) and TBA in water (solid red, 0.5M). (A) and (B) compare the solute CH band region of TBA perturbed by NaI and NaOH respectively normalized to the CH stretch, while (C) and (D) compare the solute CH band region of TBA perturbed by NaI, and NaOH respectively normalized to the CC stretch. TBA in NaI data collected by Denilson Mendes de Oliveira.

Figure 3.4 displays spectra which are normalized to the C-H and C-C stretch for both TBA in water and the TLS-spectra in order to analyze any frequency shifts. As can be seen, there is a significant C-H stretch shift between the TBA in water and the perturbed TBAs by both salts, while the C-C stretch of the TLS-spectrum of perturbed TBA by NaOH is shifted more than the TLS-spectrum of perturbed TBA by NaI. The average frequency difference of the CH stretch (2820-2075 cm^{-1}) of the perturbed TBAs by both salts is remarkably similar, where TBA perturbed by NaI versus TBA in water shows a red shift $\Delta\omega_{CH}$= -10.9 cm^{-1}, while the perturbed TBAs by NaOH versus TBA in water show a very similar red shift $\Delta\omega_{CH}$= -10.3 cm^{-1}. The C-C stretch of both salts, on the other hand, significantly varies with TBA perturbed by NaOH blue shifted, while the perturbed TBAs by NaI show no shift. The average frequency difference of the C-C stretch of perturbed TBAs by NaI versus TBA in water show a negligible shift of $\Delta\omega_{CC}$= -0.1 cm^{-1}, while

the average frequency difference of the C-H stretch of the perturbed TBAs by NaOH versus TBA in water show a significant blue shift $\Delta\omega_{CC}$= 14.0 cm^{-1}. This suggests that the NaI ions reside closer to the C-H bonds of the TBA, while the few NaOH ions which penetrate into TBA's hydration-shell may reside closer to the C-C bond of the TBA. Spectra of TBA in aqueous LiOH were also collected to analyze any cation influence between the TBA and the anion, as Li is a smaller and less polarizable atom in comparison to Na.

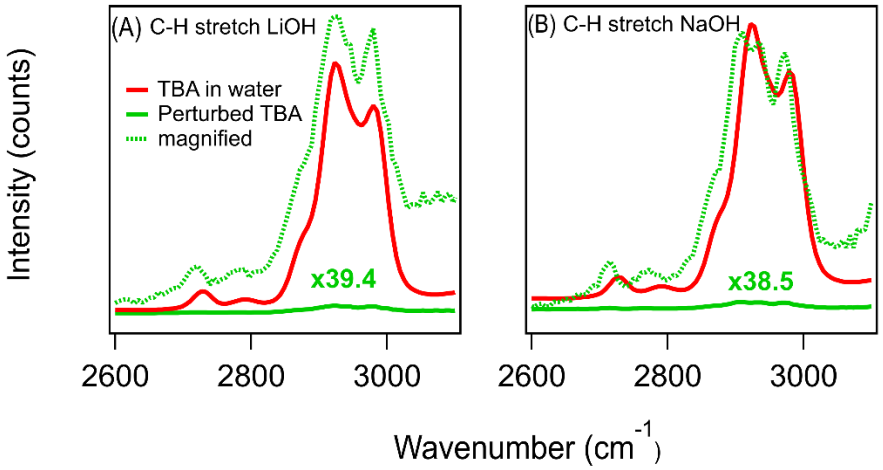

Figure 3.5 C-H band regions of the Raman-MCR SC spectra of the non-negative TLS-spectrum of TBA (0.5M) by the salts (1M) (solid green), the TLS-spectra magnified to the area of TBA in water (dashed green) and TBA in water (solid red). (A) and (B) compare the solute CH band region of TBA perturbed by LiOH and NaOH respectively.

Figure 3.5 presents the TLS spectra of the perturbed TBA in LiOH and NaOH, focused on the C-H region. Both TLS spectra of TBA in LiOH and TBA in NaOH have similar intensities, where the TBA perturbed by LiOH has a f_{CH}= 2.3%. The similar f-ratio between the two salts suggests that the change in cation does not significantly influence the hydration-shell of the TBA, which is consistent with past vibrational experiments showing little cation attraction or repulsion for the oil/water or air/water interfaces.[75-79]

3.5 Conclusion

In conclusion, NaI shows significant TBA perturbation by the salt with a large C-H stretch f-ratio, while NaOH has a much smaller C-H f-ratio at the same concentration. This small f-ratio suggests that NaOH does not penetrate as much into the hydration-shell of TBA in comparison to

NaI. However, while the number of hydroxides which do reside near the oil/water interface are small, they are measurable. While these results show that hydroxide may reside near the oil/water interface, the degree of affiliation is much more subtle in comparison to past experimental literature which attributes any negative charge accumulation near hydrophobic surfaces to hydroxide absorption.[58, 71-72] In addition to determining the affiliation for hydroxide at this oil/water interface, these results agree with past experiments which show no significant influence of the cation on the behavior of the anion near the interface.

3.6 Future work

Further work in this area would include more experimental analysis of the proton for the oil/water interface. Some theoretical studies suggest that hydronium ions are attracted to the oil-water interface[67], while other simulations show the hydronium to stay in the bulk.[68-69] While there is less experimental work on the proton at the oil/water interface, there are more studies which analyze the proton at the air/water interface. These experiments, such as vibrational sum frequency generation (SFG)[76, 80-81] and second harmonic generation (SHG)[82] spectroscopy, indicate that the proton is predominantly attracted to the air/water interface[83-84], while the few oil/water[71-72] experiments report inconclusive results. Preliminary spectra of a proton around an oily molecule were acquired with nitric acid and TBA (Appendix A, Figure A. 3), and analyzed using the same methods described in section 3.3. However, running the TLS analysis on this data was incredibly difficult due to the nitrate peak in nitric acid. The addition of co-solvents to recreate the residual is made extremely difficult by the overlapping peaks between nitric acid and the TBA. As a result, the next steps for this project would be to collect three-component spectra of TBA in aqueous hydrochloric acid, then run a TLS analysis to determine how a proton behaves near an oil/water interface.

CHAPTER 4. THE INFLUENCE OF HYDROGEN PEROXIDE ON HYDROPHOBIC HYDRATION-SHELL STRUCTURE

4.1 Abstract

The influence of hydrogen peroxide on the hydration-shell of an oily molecule, tert-butyl alcohol, is studied using Raman multi-variate curve resolution. To quantify this influence, the hydration-shell of TBA in aqueous hydrogen peroxide, aqueous sodium chloride and aqueous deuterated methanol are analyzed for shape changes in the OH stretch and compared to that of tert-butyl alcohol in water. Where the shape changes in the OH stretch region indicate structural changes of the hydration-shell around the oily molecule. It is found that tert-butyl alcohol in either aqueous sodium chloride or aqueous deuterated methanol results in a significantly perturbed hydration-shell, while the hydration-shell of tert-butyl alcohol in hydrogen peroxide remains remarkably comparable to that of tert-butyl alcohol in water. These results indicate sodium chloride and deuterated methanol disrupt the hydration-shell, while hydrogen peroxide can integrate into the hydration-shell of TBA and does not significantly influence the water structure.

4.2 Introduction

The behavior and physical properties of hydrogen peroxide have been an ongoing research topic for more than one hundred years.[85] While hydrogen peroxide has been industrialized for its disinfecting properties,[86] recent focus has shifted to the molecule's molecular structure in water and its potential use in supercooled experiments.[87] Supercooled experiments are able to contribute to phase change studies[88-89], as well as probe the behavior of various solutes at supercooled conditions related to the biological[90-91] and atmospheric[92-94] fields. However, there are still open-ended questions regarding the chemical's molecular behavior, specifically in water. While experiments and theoretical studies have compared properties such as dielectric constant[95-97] of pure hydrogen peroxide to that of pure water, as well as studied the crystalline structure of pure[98-101] and aqueous hydrogen peroxide[99-100, 102-105], the influence of hydrogen peroxide on the structure of water remains an open question.

This chapter will focus on hydrogen peroxide's influence on the hydration-shell of an oily molecule, specifically tert-butyl alcohol (TBA). Raman spectroscopy and Raman-SMCR are used

to analyze the hydration-shell of TBA in aqueous hydrogen peroxide (H_2O_2), sodium chloride (NaCl), and d-methanol (d-MeOH) at low and high concentrations. As will be discussed, the results indicate that at low concentration there are relatively small changes in the hydration-shell of TBA with hydrogen peroxide, NaCl, and d-MeOH. Yet at higher concentrations of hydrogen peroxide, NaCl, or d-MeOH the hydration-shell of TBA is significantly more perturbed by NaCl and d-MeOH in comparison to H_2O_2. These results show that the oily molecules in aqueous H_2O_2 show similar affects to the hydration-shell of TBA to that of TBA in water, which suggests H_2O_2 does not significantly disturb the water network and, instead, behaves similarly to water.

4.3 Methods

Three-component solutions of tert-butyl alcohol (TBA) in the aqueous solvents of hydrogen peroxide (H_2O_2), sodium chloride (NaCl), and deuterated methanol (d-MeOH) were prepared. TBA and NaCl were weighed, while H_2O_2 and d-MeOH were transferred volumetrically into individual 10 ml volumetric flasks and diluted to the necessary concentrations with water from a Millipore purification system (H_2O, 18.2 MΩ·cm from Milli-Q UF plus). Afterward, TBA was weighed into multiple 5ml volumetric flasks and the aqueous solvent from the previous step used to dilute the TBA to 0.5M. Each volumetric flask was inverted several times to ensure all solids were dissolved, and the solutions were then pipetted into glass cuvettes and capped.

The samples were collected at 20°C using the Raman system described in section 1.2 and analyzed to obtain the SC-spectra using the methods provided in section 1.3.

4.4 Results and Discussion

Figure 4.1 (A) displays the Raman spectra of water (dashed blue) and H_2O_2 in water solution (dotted purple), along with the solute-correlated spectra (SC-spectra) of hydrogen peroxide in water (solid purple). As can be seen, the OH stretch region (~3200-3800 cm^{-1}) of the solution in comparison to bulk water is remarkably similar, indicating the waters around hydrogen peroxide behave like bulk water. In addition, the SC-spectrum of H_2O_2 in water [Figure 4.1 (A)] reveals four peaks in the OH stretch region from ~2800-3660 cm^{-1}, which are attributed to the H_2O_2 and perturbed water molecules. More specifically, we assign the peak ~2850 cm^{-1} to the bend overtone of H_2O_2, the 3065 cm^{-1} and 3225 cm^{-1} peaks to the hydrogen

bonds of H_{H2O2}--O_{water} and H_{water}--O_{water}, respectively, and the high frequency 3540 cm^{-1} peak to the H_{water}---O_{H2O2} bond. The peaks from ~1200-1800 cm^{-1} are assigned to the bend vibrations of the waters around H_2O_2, along with the bend vibrations of H_2O_2. The peak at 1640 cm^{-1} is slightly shifted from that of pure water and is assigned to the bend vibrations of water in the hydration-shell of H_2O_2, while the ~1460 cm^{-1} peak is associated with the bend vibrations of H_2O_2. Finally, the peak at ~876 cm^{-1} belongs to the OO stretch of the hydrogen peroxide. The in-depth analyses of the assignments for these peaks is further described in a forthcoming published paper. The following chapter will instead focus on the results of H_2O_2 influence on the hydrophobic hydration-shell.

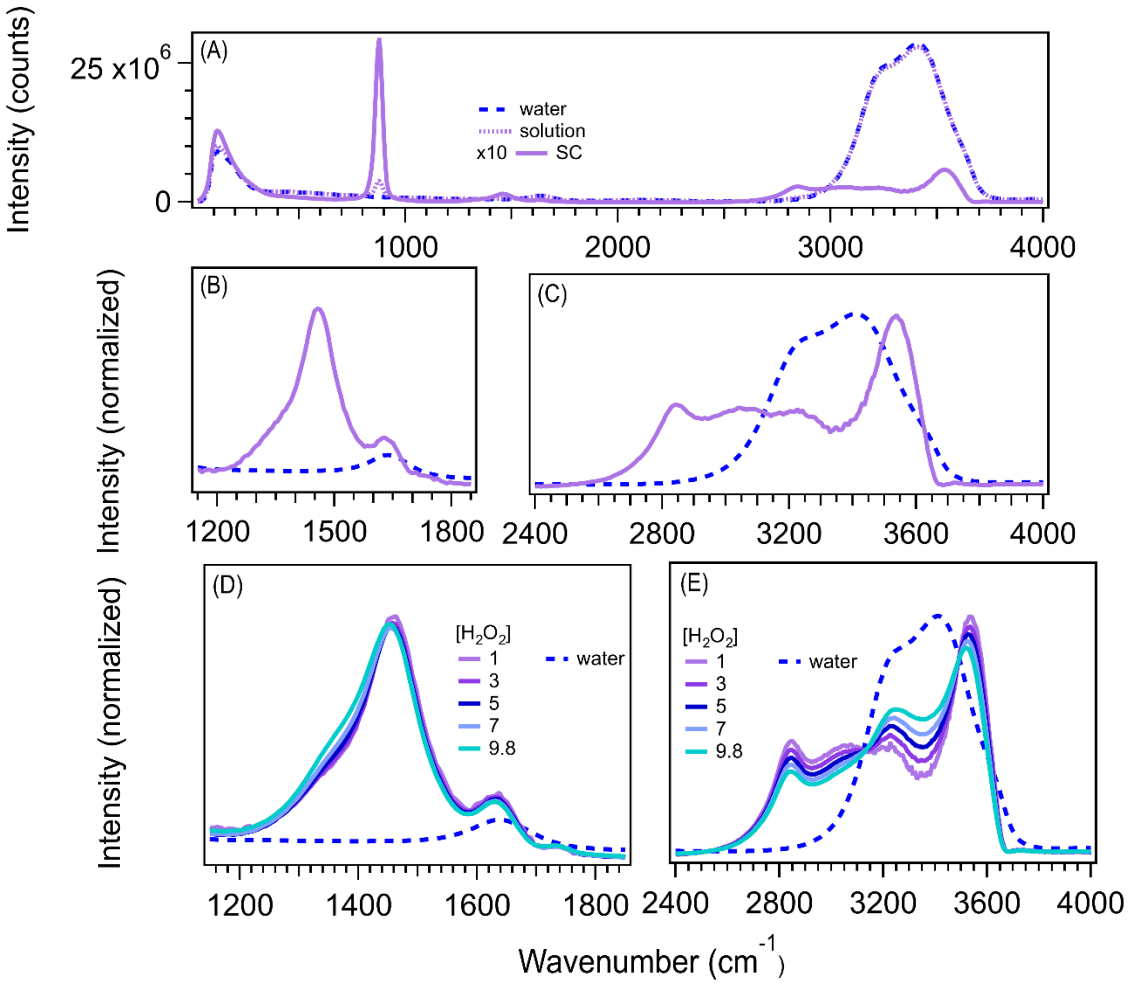

Figure 4.1 (A)-(C) are Raman spectra of pure water and hydrogen peroxide in water along with Raman-MCR of hydrogen peroxide in water (1M). (B) focuses on the OH bend region and (C) focuses on the OH stretch region. (D) and (E) show concentration-dependent SC spectra of H_2O_2 bend and stretch regions, respectively, along with water (blue, dashed) where (B)-(E) are normalized to the OH stretch region and the bend regions (B) and (D) are magnified by a factor of four. (D)-(E) collected by Denilson Mendes de Oliveira).

To determine the influence of H_2O_2 on the hydrophobic hydration-shell, the hydration-shell of TBA in aqueous H_2O_2, NaCl, and d-MeOH at both low and high concentrations were compared to TBA in water. NaCl and d-MeOH were chosen because both molecules are relatively similar in size to H_2O_2 and are soluble in water up to the relevant concentrations. While these molecules are similar in these aspects, their influences on the hydration-shell are surprisingly different in comparison to H_2O_2.

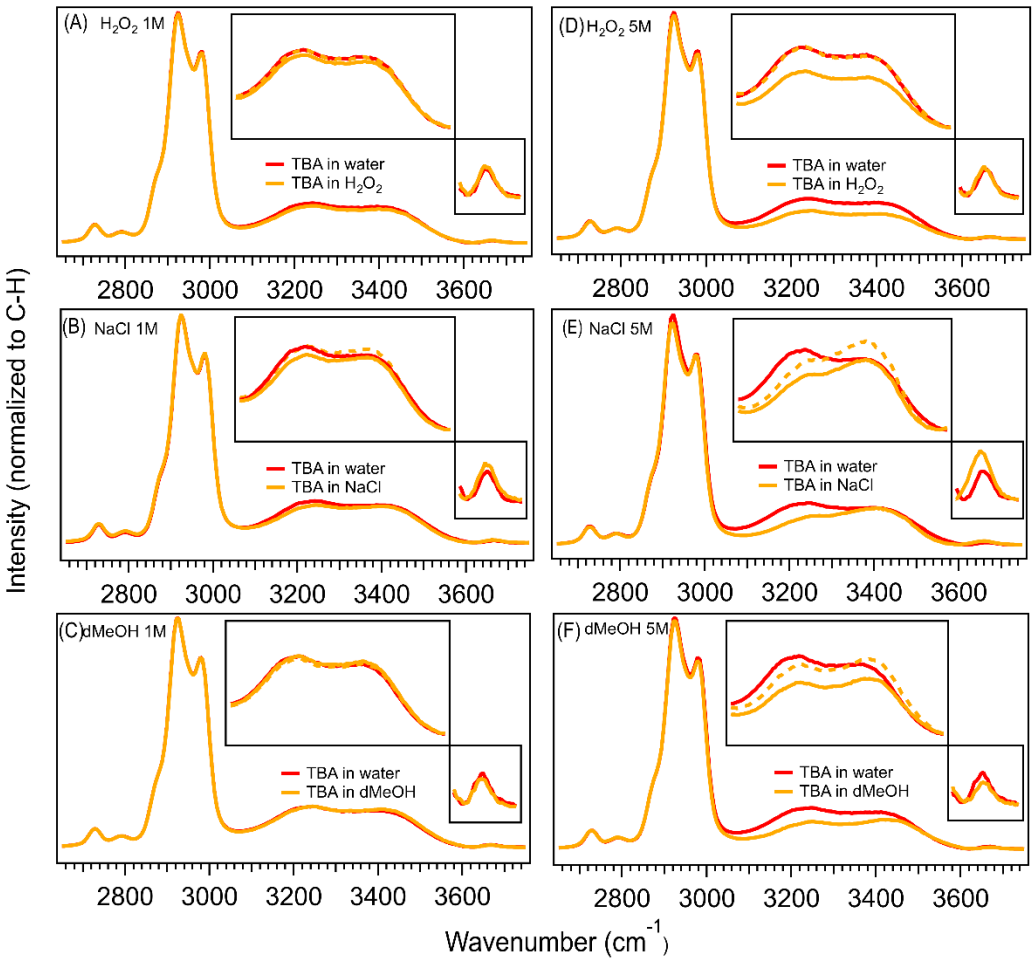

Figure 4.2 Comparison of the TBA hydration-shell in water versus aqueous (A) and (D) H_2O_2, (B) and (E) NaCl, and (C) and (F) d-MeOH at (A)-(C) low (1M), and (D)-(F) high (5M) concentration. The two inset panels are expanded views of the OH stretch [upper left for (A)-(F)] and the dangling OH stretch [lower right for (A)-(F)]. Data for d-MeOH were collected by Denilson Mendes de Oliveira.

As can be seen in Figure 4.2, the hydration-shell SC-spectrum of TBA in water (solid red) is compared with TBA in aqueous H_2O_2, NaCl, and d-MeOH (solid orange) at low concentration (1M) and high concentration (5M). The inset panels focus on the OH stretch and contain magnified spectra, where the area of the OH stretch (~3070-3620 cm^{-1}) of TBA in aqueous H_2O_2, NaCl, and d-MeOH is equal to the OH stretch area of TBA in water (dashed orange). The hydration-shell shape between TBA in water versus the three component mixture is more difficult to ascertain at low concentrations [Figure 4.2 (A)-(C)]. As can be seen at low concentration, the H_2O_2 and d-MeOH spectra show the least amount of shape change in the hydration-shell, while the NaCl (B) shows a subtle increase in the high frequency shoulder of the OH stretch. The high concentration

spectra [Figure 4.2 (D)-(F)], on the other hand, magnify and better display shape changes of the OH stretch in comparison to the low concentration spectra. What is most noticeable and surprising is that while the area of the OH stretch decreases for TBA in aqueous H_2O_2 at higher concentration, the shape of the OH stretch remains remarkably similar to that of TBA in water [Figure 4.2 (D)]. The depletion of the OH stretch is consistent and expected as water molecules are replaced with H_2O_2 in the solution. What is unexpected is the consistent OH shape which indicates H_2O_2 is not disrupting the structure of the remaining waters around TBA, a direct contrast to the other molecules at the same concentration.

The OH stretch in aqueous NaCl and d-MeOH [Figure 4.2 (E)-(F)], on the other hand, shows depletion as well as significant differences in shape. Both NaCl and d-MeOH show an average OH stretch shift to higher frequency, $\Delta\omega$ = -11 cm^{-1} and $\Delta\omega$ = -14 cm^{-1}, respectively, in comparison to TBA in water, where the average OH stretch was calculated from 3200-3800 cm^{-1} using equation (1) from section 2.4. This average OH stretch shift reveals the NaCl and d-MeOH influence on the structure of the remaining waters around TBA. Furthermore, the decrease in intensity on the low frequency peak around 3200 cm^{-1} is indicative of a decrease in tetrahedrality of the hydration-shell of TBA.[106-107] In addition to the OH stretch, the dangling OH stretch (located ~3660 cm^{-1}) also shows NaCl and d-MeOH further influencing the hydration-shell of TBA.[36, 108]

The dangling OH stretch (~ 3660 cm^{-1}) of the high concentration spectra for NaCl and d-MeOH [Figure 4.2 (E)-(F) bottom right inset panel] both show changes in intensity in comparison to the dangling OH of TBA in water. The increase in the dangling OH intensity for NaCl implies the ions of the molecule disrupt the hydration-shell around TBA and increase the number of dangling OH water molecules. The decrease in intensity of the dangling OH stretch of d-MeOH indicates that as the concentration of d-MeOH increases, the number of dangling water molecules is reduced as the dangling water molecules are displaced by the d-MeOH. The intensity of the dangling OH stretch of H_2O_2 [Figure 4.2 (D) bottom right inset panel], on the other hand, remains unchanged in comparison to TBA in water, which suggests that even though the water molecules around TBA are being displaced by H_2O_2, the change does not influence the number of dangling waters molecules.

In addition to first round SMCR, total least squares (TLS) was used to determine the non-negative residual spectra as described in section 1.3.2.

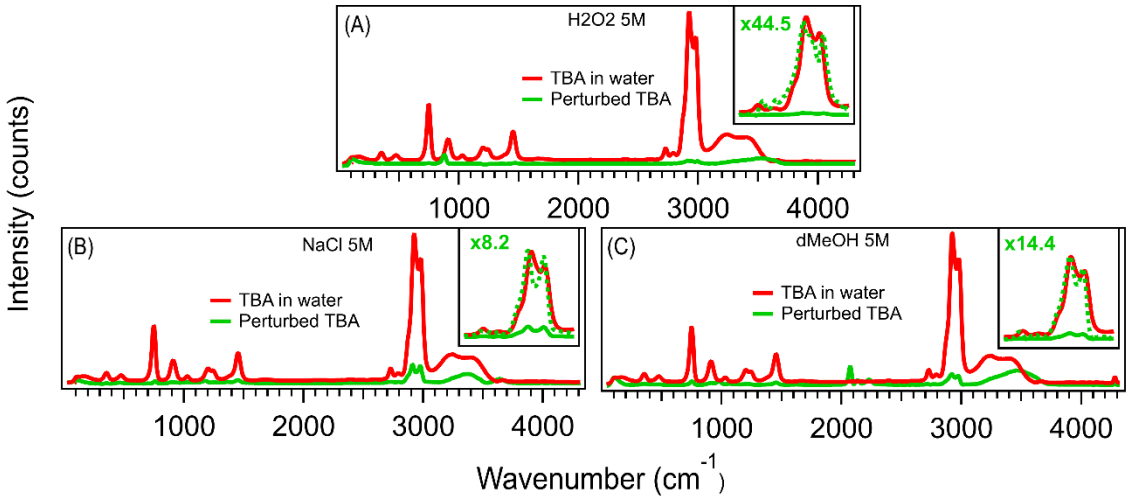

Figure 4.3 (A)-(C) TLS-spectra of TBA (0.5M) in water (solid red) and TBA (0.5M) perturbed by aqueous H_2O_2, NaCl and d-MeOH (5M) respectively (solid green). The inset panels include a magnified CH stretch (dashed green) equal to the same CH stretch area of TBA in water. Data for panel (C) was collected by Denilson Mendes de Oliveira.

Figure 4.3 shows the TLS-spectra of TBA in water (solid red) and the non-negative spectra residual of TBA in aqueous H_2O_2, NaCl, and d-MeOH (solid green) at the higher concentration (5M). The residual is the amount of TBA which is perturbed by H_2O_2, NaCl, and d-MeOH. Table 4.1 displays the resulting CH stretch f-ratios, where the f-ratio is the fraction of TBA perturbed by the aqueous molecules divided by that of the total interactions in the solution, calculated by

$$f = \frac{A_I}{A_T} = \frac{I_{TLS}}{I_{TBA}+I_{TLS}} \qquad \text{(I)}$$

where the CH stretch area of perturbed TBA (A_I) is divided by the CH stretch area of the total interactions of the CH stretch (A_T). The f-ratio produced by the various high concentration (5M) salts (Table 4.1) again shows little perturbation of TBA by H_2O_2, with an f_{CH}= 2% remarkably similar to the fraction of perturbed TBA by H_2O_2 at low concentration (1M). Both NaCl and d-MeOH, on the other hand, show significant perturbation of TBA with f_{CH}= 11% and f_{CH}= 6% respectively. This fraction of perturbed TBA is also reflected in the inset panels of Figure 4.3 (A)-(C) where the perturbed TBA is magnified to the area of TBA in water, and shows H_2O_2 perturbing TBA less than either NaCl or d-MeOH. These results indicate that H_2O_2 integrates into the hydration-shell of the oily molecule and does not significantly perturb the surrounding water

molecules as opposed to NaCl and d-MeOH which penetrate the hydration-shell and disrupt the water structure.

Table 4.1 Comparison of the C-H stretch f-ratio of TBA perturbed by high (5M) concentration of aqueous salt.

Solvent	CH f-ratio (5M)
H_2O_2	0.0219554
NaCl	0.108378
d-MeOH	0.0647604

4.5 Conclusion

In conclusion, H_2O_2 does not show signs of influencing the hydration-shell of an oil molecule and instead integrates into the hydrogen bonding network and behaves similarly to water. At high concentrations, where the OH stretch depletes and water molecules are replaced with H_2O_2, the shape remains remarkably like TBA in water. Furthermore, the dangling OH stretch also remains relatively unchanged, suggesting that the number of dangling OH groups remain the same despite the increase in H_2O_2 concentration. This is in direct contrast to NaCl and d-MeOH, where both molecules show significant influence on the hydration-shell of TBA, with the OH stretch depletion and shape change indicating a loss in tetrahedrality of the hydration-shell. These molecules, as opposed to H_2O_2, also affect the number of dangling OH groups, with NaCl and d-MeOH having opposite effects, with NaCl increasing and d-MeOH decreasing the number of OH groups around TBA. Furthermore, the TLS-spectra indicate NaCl and d-MeOH significantly perturb TBA, while H_2O_2 shows little perturbation at the relatively high concentration. These results suggest that H_2O_2 behaves similarly to water and does not significantly alter the hydrogen bonding network of the hydration-shell. This feature could be of use to those studying solutes at low temperature, as H_2O_2 could be used as an additional cooling agent.

4.6 Future work

This work shows that H_2O_2 can integrate into the hydrogen bonding network and leave the hydration-shell water structure relatively unaffected. As past experiments have shown, H_2O_2 has the potential to reach supercooled temperatures, allowing future work using hydrogen peroxide to include studies related to supercooled experiments. Extending experiments to supercooled

temperatures is important in answering a variety of questions, from natural anti-freeze properties to investigating potential low temperature hydration-shell crossovers.[90, 109] While H_2O_2 can reach supercooled temperatures and does not seem to influence the hydration-shell of oily molecules, more research must be conducted to explore any inhibited properties, such as density between supercooled water and aqueous H_2O_2.[110-111]

APPENDIX A. ADDITIONAL ION AFFILIATION SPECTRA

The following are additional spectra collected using the same methods described in section 3.3 of TBA in aqueous NaCl and LiCl.

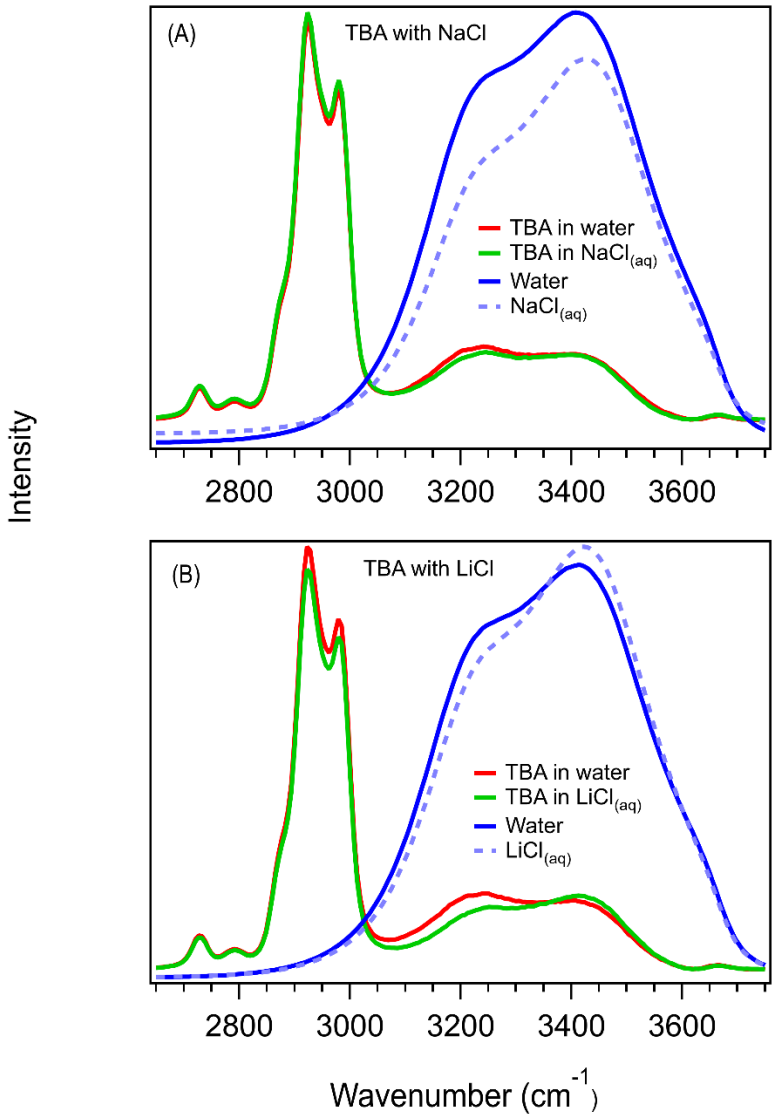

Figure A. 1 Raman-MCR SC spectra in the solute CH and hydration-shell OH band regions. (A) and (B) compare the SC spectrum of TBA in NaCl (solid green trace) versus TBA in LiCl (solid green trace) both normalized to the CH stretch. Where the solid red trace is TBA in water, the solid blue trace is water, and the dashed light-blue trace is the aqueous salt (NaCl and LiCl respectively).

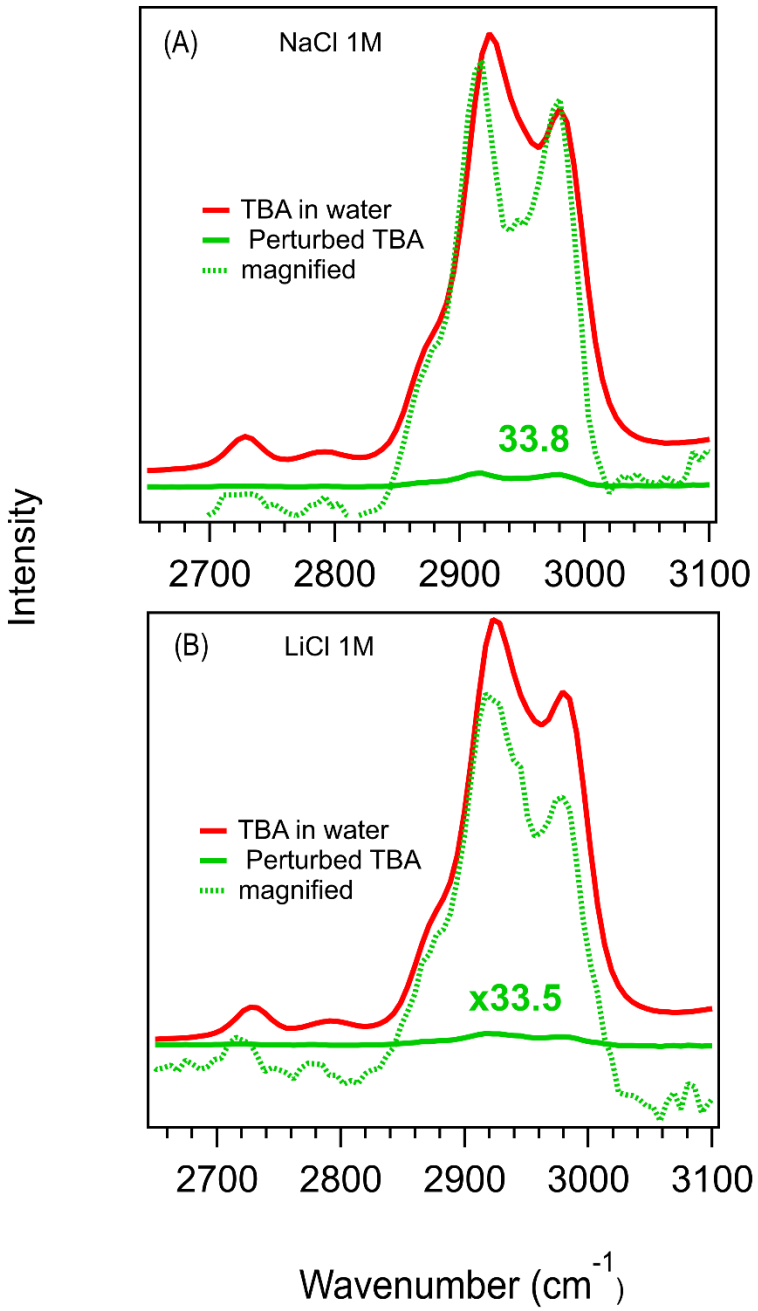

Figure A. 2 C-H band regions of the Raman-MCR SC-spectra of the non-negative TLS-spectrum of TBA by the salts (solid green), the TLS-spectra magnified to the area of TBA in water (dashed green) and TBA in water (solid red). (A) and (B) compare the solute CH band region of TBA perturbed by NaCl versus LiCl, respectively.

The following are preliminary SC and TLS spectra of TBA in aqueous nitric acid.

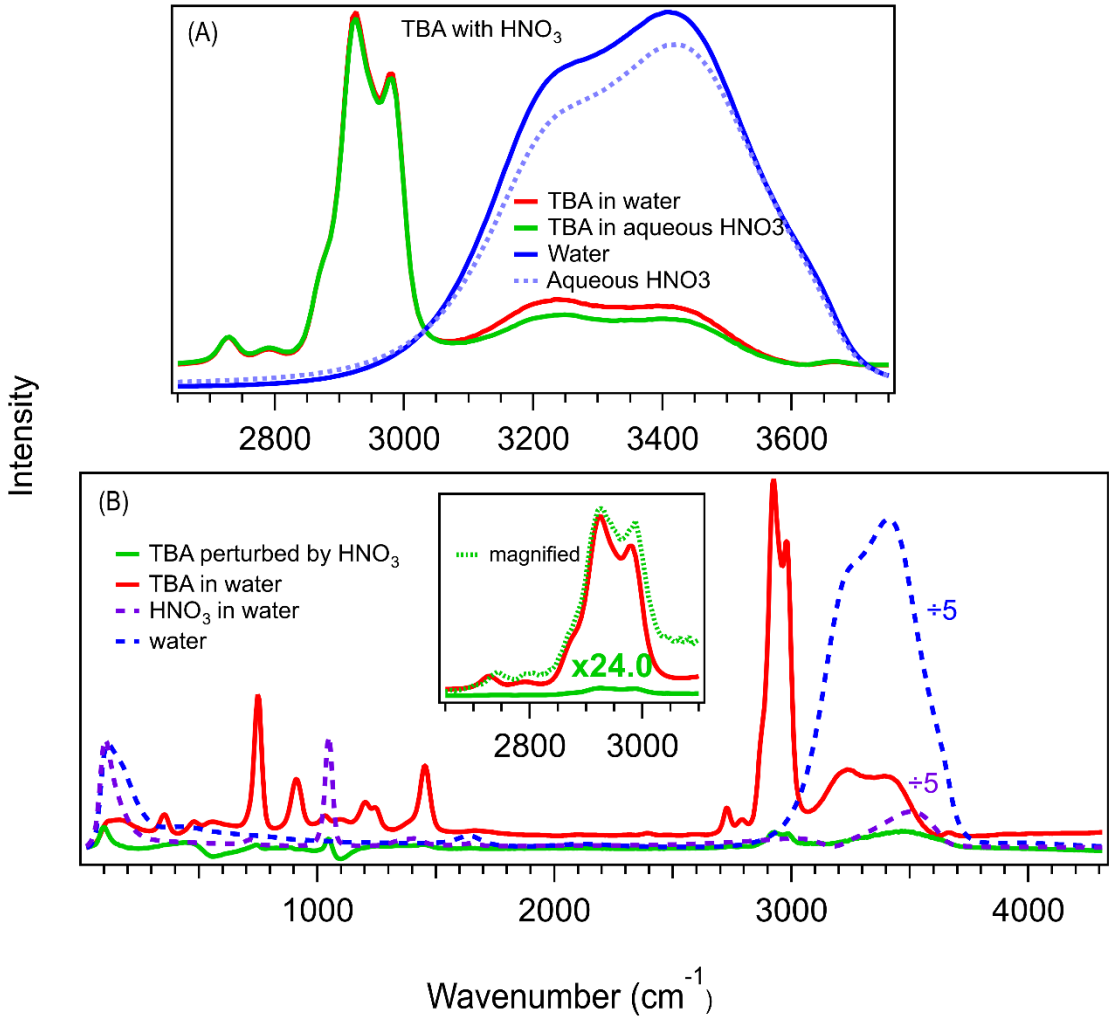

Figure A. 3 (A) Raman-MCR SC-spectra in the solute's CH and hydration-shell OH band regions. Where the solid green trace is TBA in HNO_3, solid red trace is TBA in water, the solid blue trace is water, and the dashed light-blue trace is aqueous HNO_3. (B) Raman-MCR SC-spectra of TBA in water (solid red), salt in water (dashed purple), and water (dashed blue curve) as well as the non-negative TLS-spectrum of TBA by HNO_3 (solid green). The inset panel contains the TLS-spectrum magnified to the area of TBA in water (dashed green).

The following are preliminary SC and TLS spectra of TBA in aqueous sodium nitrate.

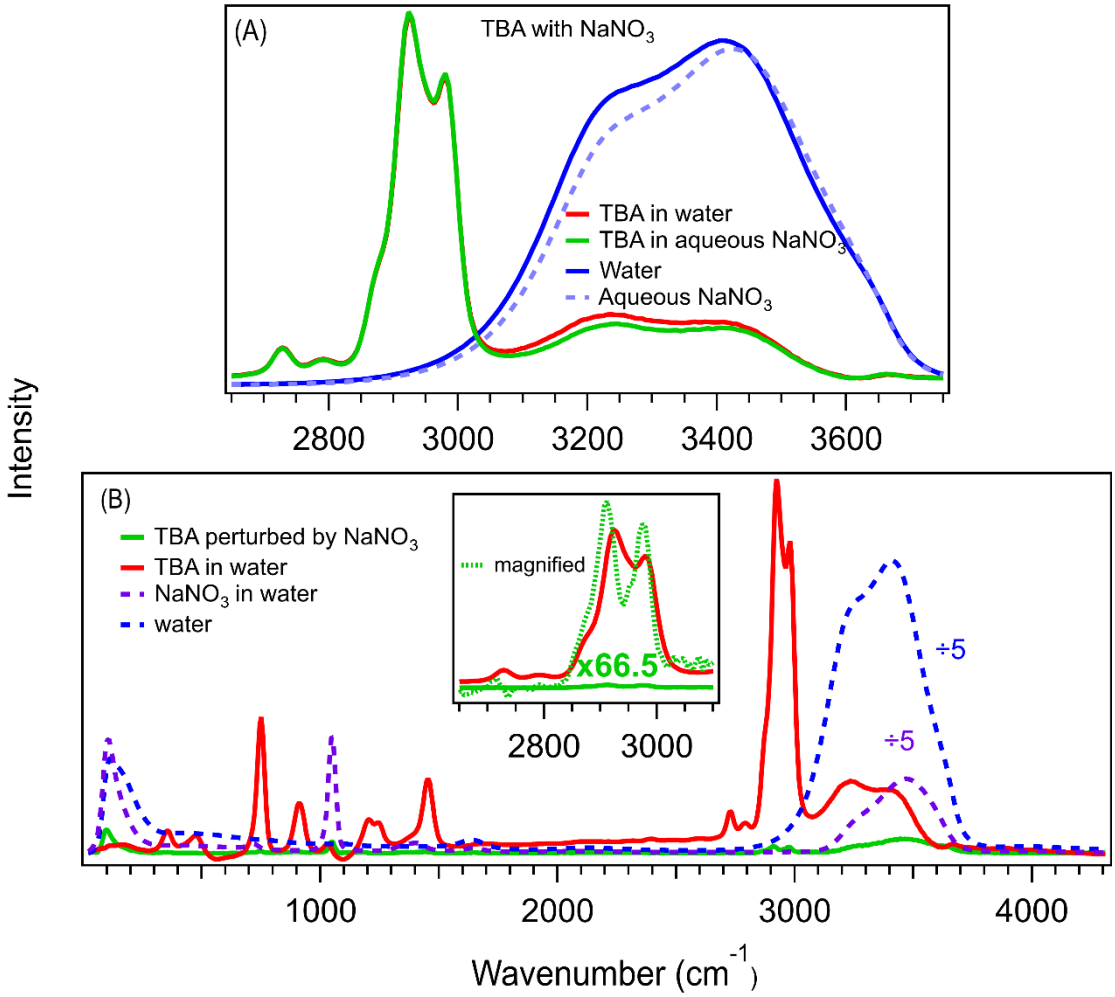

Figure A. 4 (A) Raman-MCR SC spectra in the solute's CH and hydration-shell OH band regions. Where the solid green trace is TBA in $NaNO_3$, solid red trace is TBA in water, the solid blue trace is water, and the dashed light-blue trace is aqueous $NaNO_3$. (B) Raman-MCR SC-spectra of TBA in water (solid red), salt in water (dashed purple), and water (dashed blue curve) as well as the non-negative TLS-spectrum of TBA by $NaNO_3$ (solid green). The inset panel contains the TLS-spectrum magnified to the area of TBA in water (dashed green).

APPENDIX B. ADDITIONAL SPECTRA FOR HYDROGEN PEROXIDE INFLUENCE ON HYDRATION-SHELL

The following is an additional figure for chapter 4. It contains SC-spectra of H_2O_2 in water, d-MeOH in water as well as TLS-spectra of TBA perturbed by H_2O_2 and TBA perturbed by d-MeOH focused in the OO stretch region and CD stretch region.

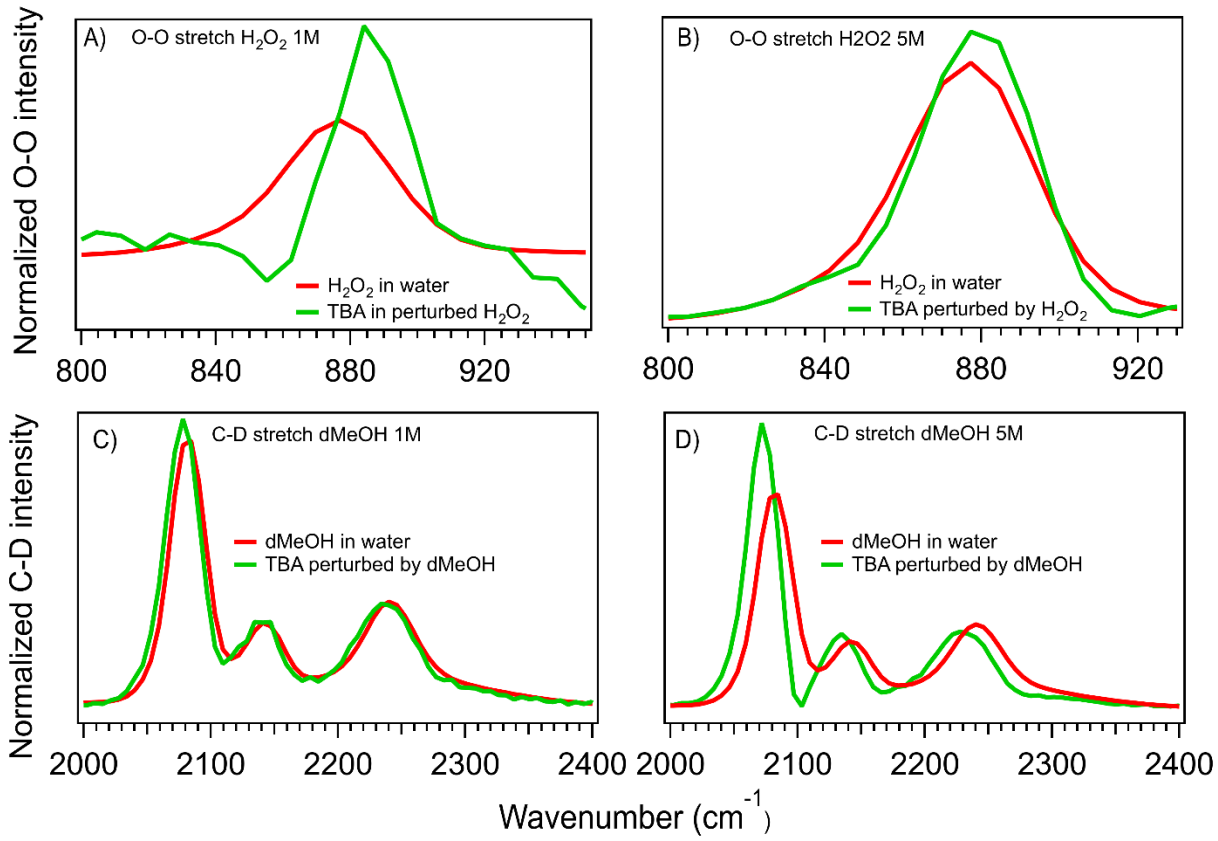

Figure B. 1 O-O and C-D band regions of the non-negative TLS-spectrum of TBA perturbed by H_2O_2 and TBA perturbed by d-MeOH (solid green) as well as TBA in water (solid red). (A) and (B) compare the solute O-O stretch band region of TBA perturbed by H_2O_2 at low (1M) and high (5M) concentration, while (C) and (D) compare the C-D band region of TBA perturbed by d-MeOH at low (1M) and high (5M) concentration. Data for panels (C)-(D) were collected by Denilson Mendes de Oliveira.

REFERENCES

1. Davis, J. G.; Gierszal, K. P.; Wang, P.; Ben-Amotz, D., Water structural transformation at molecular hydrophobic interfaces. *Nature* **2012,** *491* (7425), 582-5.

2. Gierszal, K. P.; Davis, J. G.; Hands, M. D.; Wilcox, D. S.; Slipchenko, L. V.; Ben-Amotz, D., π-Hydrogen Bonding in Liquid Water. *The Journal of Physical Chemistry Letters* **2011,** *2* (22), 2930-2933.

3. Matt, S. M.; Ben-Amotz, D., Influence of Intermolecular Coupling on the Vibrational Spectrum of Water. *J Phys Chem B* **2018**.

4. Fega, K. R.; Wilcox, D. S.; Ben-Amotz, D., Application of Raman multivariate curve resolution to solvation-shell spectroscopy. *Appl Spectrosc* **2012,** *66* (3), 282-8.

5. Ball, P., Water as an active constituent in cell biology. *Chem. Rev.* **2008,** *108* (1), 74-108.

6. Laage, D.; Elsaesser, T.; Hynes, J. T., Water Dynamics in the Hydration Shells of Biomolecules. *Chem. Rev.* **2017,** *117* (16), 10694-10725.

7. Cabane, E.; Zhang, X. Y.; Langowska, K.; Palivan, C. G.; Meier, W., Stimuli-Responsive Polymers and Their Applications in Nanomedicine. *Biointerphases* **2012,** *7* (1-4).

8. Martins, P. A. T.; Domingues, N.; Pires, C.; Alves, A. M.; Palmeira, T.; Samelo, J.; Cardoso, R.; Velazquez-Campoy, A.; Moreno, M. J., Molecular crowding effects on the distribution of amphiphiles in biological media. *Colloid Surf. B-Biointerfaces* **2019,** *180*, 319-325.

9. Stillinger, F. H., Structure in aqueous solutions of nonpolar solutes from the standpoint of scaled-particle theory. *J. Solution Chem.* **1973,** *2*, 141-158.

10. Lum, K.; Chandler, D.; Weeks, J. D., Hydrophobicity at Small and Large Length Scales. *J. Phys. Chem. B* **1999,** *103*, 4570-4577.

11. Chandler, D., Interfaces and the driving force of hydrophobic assembly. *Nature* **2005,** *437* (7059), 640-647.

12. Rajamani, S.; Truskett, T. M.; Garde, S., Hydrophobic hydration from small to large lengthscales: Understanding and manipulating the crossover. *PNAS* **2005,** *102* (27), 9475-9480.

13. Willard, A. P.; Chandler, D., The role of solvent fluctuations in hydrophobic assembly. *J. Phys. Chem. B* **2008,** *112* (19), 6187-6192.

14. Duboue-Dijon, E.; Fogarty, A. C.; Laage, D., Temperature Dependence of Hydrophobic Hydration Dynamics: From Retardation to Acceleration. *J. Phys. Chem. B* **2014,** *118* (6), 1574-1583.

15. Hande, V. R.; Chakrabarty, S., Structural Order of Water Molecules around Hydrophobic Solutes: Length-Scale Dependence and Solute-Solvent Coupling. *J. Phys. Chem. B* **2015,** *119* (34), 11346-11357.

16. Petersen, C.; Tielrooij, K. J.; Bakker, H. J., Strong temperature dependence of water reorientation in hydrophobic hydration shells. *J. Chem. Phys.* **2009,** *130* (21), 214511.

17. Li, I. T. S.; Walker, G. C., Signature of hydrophobic hydration in a single polymer. *Proc. Natl. Acad. Sci. U. S. A.* **2011,** *108* (40), 16527-16532.

18. Li, I. T. S.; Walker, G. C., Single Polymer Studies of Hydrophobic Hydration. *Accounts Chem. Res.* **2012,** *45* (11), 2011-2021.

19. Wu, X. E.; Lu, W. J.; Streacker, L. M.; Ashbaugh, H. S.; Ben-Amotz, D., Temperature-Dependent Hydrophobic Crossover Length Scale and Water Tetrahedral Order. *J. Phys. Chem. Lett.* **2018,** *9* (5), 1012-1017.

20. Wu, X. E.; Lu, W. J.; Streacker, L. M.; Ashbaugh, H. S.; Ben-Amotz, D., Methane Hydration-Shell Structure and Fragility. *Angew. Chem.-Int. Edit.* **2018,** *57* (46), 15133-15137.

21. Mochizuki, K.; Ben-Amotz, D., Hydration-Shell Transformation of Thermosensitive Aqueous Polymers. *J. Phys. Chem. Lett.* **2017,** *8* (7), 1360-1364.

22. Bohm, F.; Schwaab, G.; Havenith, M., Mapping Hydration Water around Alcohol Chains by THz Calorimetry. *Angew. Chem.-Int. Edit.* **2017,** *56* (33), 9981-9985.

23. Lenton, S.; Rhys, N. H.; Towey, J. J.; Soper, A. K.; Dougan, L., Temperature-Dependent Segregation in Alcohol-Water Binary Mixtures Is Driven by Water Clustering. *J. Phys. Chem. B* **2018,** *122* (32), 7884-7894.

24. Soper, A. K.; Dougan, L.; Crain, J.; Finney, J. L., Excess entropy in alcohol-water solutions: A simple clustering explanation. *J. Phys. Chem. B* **2006,** *110* (8), 3472-3476.

25. Dixit, S.; Crain, J.; Poon, W. C. K.; Finney, J. L.; Soper, A. K., Molecular segregation observed in a concentrated alcohol-water solution. *Nature* **2002,** *416* (6883), 829-832.

26. Bowron, D. T.; Soper, A. K.; Finney, J. L., Temperature dependence of the structure of a 0.06 mole fraction tertiary butanol-water solution. *J. Chem. Phys.* **2001,** *114* (14), 6203-6219.

27. Ben-Amotz, D., Hydration-Shell Vibrational Spectroscopy. *J. Am. Chem. Soc.* **2019,** *141* (27), 10569-10580.

28. Gao, A.; Tan, L.; Chaudhari, M. I.; Asthagiri, D.; Pratt, L. R.; Rempe, S. B.; Weeks, J. D., Role of Solute Attractive Forces in the Atomic-Scale Theory of Hydrophobic Effects. *J. Phys. Chem. B* **2018,** *122* (23), 6272-6276.

29. Ben-Amotz, D., Water-Mediated Hydrophobic Interactions. *Ann. Rev. Phys. Chem.* **2016,** *67* (1), 617-638.

30. Wilcox, D. S.; Rankin, B. M.; Ben-Amotz, D., Distinguishing Aggregation from Random Mixing in Aqueous t-Butyl Alcohol Solutions. *Faraday Disc.* **2013,** *167* (1), 177-190.

31. Rankin, B. M.; Ben-Amotz, D.; van der Post, S. T.; Bakker, H. J., Contacts Between Alcohols in Water Are Random Rather than Hydrophobic. *J. Phys. Chem. Lett.* **2015,** *6* (4), 688-692.

32. Pattenaude, S. R.; Rankin, B. M.; Mochizuki, K.; Ben-Amotz, D., Water-mediated aggregation of 2-butoxyethanol. *Phys. Chem. Chem. Phys.* **2016,** *18* (36), 24937-24943.

33. Muller, N., Search for a Realistic View of the Hydrophobic Effect. *Acc. Chem. Res.* **1990,** *23*, 23-28.

34. Perera, P.; Wyche, M.; Loethen, Y.; Ben-Amotz, D., Solute-Induced Perturbations of Solvent-Shell Molecules Observed Using Multivariate Raman Curve Resolution. *J. Am. Chem. Soc.* **2008,** *130* (14), 4576-4577.

35. Perera, P. N.; Fega, K. R.; Lawrence, C.; Sundstrom, E. J.; Tomlinson-Phillips, J.; Ben-Amotz, D., Observation of water dangling OH bonds around dissolved nonpolar groups. *PNAS* **2009,** *106*, 12230-12234.

36. Davis, J. G.; Rankin, B. M.; Gierszal, K. P.; Ben-Amotz, D., On the cooperative formation of non-hydrogen bonded water at molecular hydrophobic interfaces. *Nat. Chem.* **2013,** *5*, 796-802.

37. Du, Q.; Freysz, E.; Shen, Y. R., Surface Vibrational Spectroscopic Studies of Hydrogen-Bonding and Hydrophobicity. *Science* **1994,** *264* (5160), 826-828.

38. Tomlinson-Phillips, J.; Davis, J.; Ben-Amotz, D.; Spangberg, D.; Pejov, L.; Hermansson, K., Structure and Dynamics of Water Dangling OH Bonds in Hydrophobic Hydration Shells. Comparison of Simulation and Experiment. *J. Phys. Chem. A* **2011,** *115* (23), 6177-6183.

39. Plyasunov, A. V.; Plyasunov, N. V.; Shock, E. L. *The database for the thermodynamic properties of neutral compounds in the state of aqueous solution*; Department of Geological Sciences, Arizona State University, Tempe AZ 85287: 2005.

40. Errington, J. R.; Debenedetti, P. G., Relationship between structural order and the anomalies of liquid water. *Nature* **2001,** *409* (6818), 318-321.

41. Sloan, E. D., *Clathrate Hydrates of Natural Gases*. Marcel Dekker:: New York, 1998.

42. Watanabe, K.; Andersen, H. C., Molecular-Dynamics Study of the Hydrophobic Interaction in an Aqueous-Solution of Krypton. *J. Phys. Chem.* **1986,** *90* (5), 795-802.

43. TenWolde, P. R.; Chandler, D., Drying-induced hydrophobic polymer collapse. *Proc. Nat. Acad. Sci. USA* **2002,** *99* (10), 6539-6543.

44. Tavagnacco, L.; Zaccarelli, E.; Chiessi, E., On the molecular origin of the cooperative coil-to-globule transition of poly(N-isopropylacrylamide) in water. *Phys. Chem. Chem. Phys.* **2018,** *20* (15), 9997-10010.

45. Long, J. A.; Rankin, B. M.; Ben-Amotz, D., Micelle Structure and Hydrophobic Hydration. *J. Am. Chem. Soc.* **2015,** *137* (33), 10809-10815.

46. Ben-Naim, A., *Solvation thermodynamics*. Plenum Press: New York, 1987.

47. Davis, J. G.; Zukowski, S. R.; Rankin, B. M.; Ben-Amotz, D., Influence of a Neighboring Charged Group on Hydrophobic Hydration Shell Structure. *J. Phys. Chem. B* **2015,** *119* (29), 9417−9422.

48. Hess, B.; Kutzner, C.; van der Spoel, D.; Lindahl, E., GROMACS 4: Algorithms for highly efficient, load-balanced, and scalable molecular simulation. *J. Chem. Theory Comput.* **2008,** *4* (3), 435-447.

49. Chen, B.; Potoff, J. J.; Siepmann, J. I., Monte Carlo calculations for alcohols and their mixtures with alkanes. Transferable potentials for phase equilibria. 5. United-atom description of primary, secondary, and tertiary alcohols. *J. Phys. Chem. B* **2001,** *105* (15), 3093-3104.

50. Abascal, J. L. F.; Vega, C., A general purpose model for the condensed phases of water: TIP4P/2005. *J. Chem. Phys.* **2005,** *123* (23).

51. Kunz, W.; Henle, J.; Ninham, B. W., 'Zur Lehre von der Wirkung der Salze' (about the science of the effect of salts): Franz Hofmeister's historical papers. *Current Opinion in Colloid & Interface Science* **2004,** *9* (1-2), 19-37.

52. Debye, P. H., Erich (1923). The theory of electrolytes. I. Freezing point depression and related phenomena [Zur Theorie der Elektrolyte. I. Gefrierpunktserniedrigung und verwandte Erscheinungen]. *Physikalische Zeitschrift. 24,* 185–206 Translated and typeset by Michael J. Braus (2020).

53. Pockels, A., On the Relative Contamination of the Water-Surface by Equal Quantities of Different Substances. *Nature* **1892,** *46*, 418-419.

54. Rayleigh, F. R. S., XXXVI. Investigations in Capillarity:—The size of drops.—The liberation of gas from supersaturated solutions.—Colliding jets.—The tension of contaminated water-surfaces. *Phil. Mag.* **1899,** *48* (293), 321-337.

55. Milner, S. R., IV. On surface concentration, and the formation of liquid films. *The London, Edinburgh, and Dublin Philosophical Magazine and Journal of Science* **1907,** *13* (73), 96-110.

56. Wagner, C., *Phys. Z.* **1924,** *25*, 474-477.

57. Onsager, L.; Samaras, N. N. T., The Surface Tension of Debye-Hückel Electrolytes. *The Journal of Chemical Physics* **1934,** *2* (8), 528-536.

58. Marinova, K. G.; Alargova, R. G.; Denkov, N. D.; Velev, O. D.; Petsev, D. N.; Ivanov, I. B.; Borwankar, R. P., Charging of Oil-Water Interfaces Due to Spontaneous Adsorption of Hydroxyl Ions. *Langmuir* **1996,** *12* (8), 2045-2051.

59. Markovich, G.; Giniger, R.; Levin, M.; Cheshnovsky, O., Photoelectron spectroscopy of iodine anion solvated in water clusters. *The Journal of Chemical Physics* **1991,** *95* (12), 9416-9419.

60. Gu, X. J.; Levandier, D. J.; Zhang, B.; Scoles, G.; Zhuang, D., On the infrared spectroscopy of SiF4 and SF6 in Ar clusters: Location of the solute. *The Journal of Chemical Physics* **1990,** *93* (7), 4898-4906.

61. Grinnell Jones; Ray, W. A., The Surface Tension of Solutions of Electrolytes as a Function of the Concentration II. *J. Am. Chem. Soc.* **1941,** *63* (1), 288-294.

62. Peter K. Weissenborn; Pugh, R. J., Surface Tension and Bubble Coalescence Phenomena of Aqueous Solutions of Electrolytes. *Langmuir* **1995,** *11*, 1422-1426.

63. Levin, Y., Polarizable ions at interfaces. *Phys Rev Lett* **2009,** *102* (14), 147803.

64. Ball, P., Water as an active constituent in cell biology. *chemical Reviews* **2008,** *108*.

65. Krebs, T.; Schroën, C. G. P. H.; Boom, R. M., Separation kinetics of an oil-in-water emulsion under enhanced gravity. *Chemical Engineering Science* **2012,** *71*, 118-125.

66. Wang, X.; Qiu, X.; Wu, C., Comparison of the Coil-to-Globule and the Globule-to-Coil Transitions of a Single Poly(N-isopropylacrylamide) Homopolymer Chain in Water. *Macromolecules* **1998,** *31* (9).

67. Va´cha, R.; Horinek, D.; Berkowitzc, M. L.; Jungwirth, P., Hydronium and hydroxide at the interface between water and hydrophobic media. *Phys Chem Chem Phys* **2008,** *10* (32), 4676-7.

68. Kudin, K. N.; Car, R., Why Are Water-Hydrophobic Interfaces Charged? *American Chemical Society* **2008,** *130* (3915-3919).

69. Zangi, R.; Engberts, J. B. F. N., Physisorption of Hydroxide Ions from Aqueous Solution to a Hydrophobic Surface. *American Chemical Society* **2005,** *127*.

70. Beattie, J. K.; Djerdjev, A. M., The pristine oil/water interface: surfactant-free hydroxide-charged emulsions. *Angew Chem Int Ed Engl* **2004,** *43* (27), 3568-71.

71. Patrice Creux; Jean Lachaise; Alain Graciaa; James K. Beattie; Djerdjev, A. M., Strong Specific Hydroxide Ion Binding at the Pristine Oil/Water and Air/Water Interfaces. *J. Phys. Chem. B* **2009,** *113*, 14146-14150.

72. Tian, C. S.; Shen, Y. R., Structure and charging of hydrophobic material/water interfaces studied by phase-sensitive sum-frequency vibrational spectroscopy. *Proceedings of the National Academy of Sciences of the United States of America* **2009,** *106* (36), 15148-15153.

73. Fang, H.; Wu, W.; Sang, Y.; Chen, S.; Zhu, X.; Zhang, L.; Niu, Y.; Gan, W., Evidence of the adsorption of hydroxide ion at hexadecane/water interface from second harmonic generation study. *RSC Advances* **2015,** *5* (30), 23578-23585.

74. Rankin, B. M.; Hands, M. D.; Wilcox, D. S.; Fega, K. R.; Slipchenko, L. V.; Ben-Amotz, D., Interactions between halide anions and a molecular hydrophobic interface. *Faraday Discuss.* **2013,** *160*, 255-270.

75. Rankin, B. M.; Ben-Amotz, D., Expulsion of ions from hydrophobic hydration shells. *J Am Chem Soc* **2013,** *135* (24), 8818-21.

76. Teresa L. Tarbuck; Stephanie T. Ota; Richmond, G. L., Spectroscopic Studies of Solvated Hydrogen and Hydroxide Ions at Aqueous Surfaces. *J. AM. CHEM. SOC.* **2006,** *128*, 14519-14527.

77. Lilley, T. H., Raman Spectroscopy of Aqueous Electrolyte Solutions. In *Aqueous Solutions of Simple Electrolytes*, Franks, F., Ed. Springer: New York, NY, 1973; Vol. 3, pp 265-299.

78. Cacace, M. G.; Landau, E. M.; Ramsden, J. J., The Hofmeister series: salt and solvent effects on interfacial phenomena. *Q Rev Biophys* **1997,** *30* (3), 241-77.

79. Perera, P. N.; Browder, B.; Ben-Amotz, D., Perturbations of Water by Alkali Halide Ions Measured using Multivariate Raman Curve. *J. Phys. Chem. B* **2009,** *113* (7).

80. Chiang, K. Y.; Dalstein, L.; Wen, Y. C., Affinity of Hydrated Protons at Intrinsic Water/Vapor Interface Revealed by Ion-Induced Water Alignment. *J Phys Chem Lett* **2020,** *11* (3), 696-701.

81. Lori M. Levering; M. Roxana Sierra-Herna´ndez; Allen, H. C., Observation of Hydronium Ions at the Air-Aqueous Acid Interface: Vibrational Spectroscopic Studies of Aqueous HCl, HBr, and HI. *J. Phys. Chem. C* **2007,** *111* (25), 8814-8826.

82. Poul B. Petersen; Saykally, R. J., Evidence for an Enhanced Hydronium Concentration at the Liquid Water Surface. *J. Phys. Chem. B* **2005,** *109*, 7976-7980.

83. Agmon, N.; Bakker, H. J.; Campen, R. K.; Henchman, R. H.; Pohl, P.; Roke, S.; Thamer, M.; Hassanali, A., Protons and Hydroxide Ions in Aqueous Systems. *Chem Rev* **2016,** *116* (13), 7642-72.

84. Buch, V.; Milet, A.; Vacha, R.; Jungwirth, P.; Devlin, J. P., Water surface is acidic. *Proc Natl Acad Sci U S A* **2007,** *104* (18), 7342-7.

85. O. Maass; Herzberg, O. W., THE PROPERTIES OF PURE HYDROGEN PEROXIDE. II. *American Chemical Society* **1920,** *42* (12), 2569-2570.

86. W.C. Schumb; C.N. Satterfield; Wentworth, R. L., Hydrogen Peroxide Part two. Research, O. o. N., Ed. Document Service Center: Massachusetts Institute of Technology, 1953.

87. K. A. COOPER; WATKINSON, J. G., The Supercooling of Aqeous Hydrogen Peroxide. *Transactions of the Faraday Society* **1957,** *53*, 635-641.

88. Sellberg, J. A.; Huang, C.; McQueen, T. A.; Loh, N. D.; Laksmono, H.; Schlesinger, D.; Sierra, R. G.; Nordlund, D.; Hampton, C. Y.; Starodub, D.; DePonte, D. P.; Beye, M.; Chen, C.; Martin, A. V.; Barty, A.; Wikfeldt, K. T.; Weiss, T. M.; Caronna, C.; Feldkamp, J.; Skinner, L. B.; Seibert, M. M.; Messerschmidt, M.; Williams, G. J.; Boutet, S.; Pettersson, L. G.; Bogan, M. J.; Nilsson, A., Ultrafast X-ray probing of water structure below the homogeneous ice nucleation temperature. *Nature* **2014,** *510* (7505), 381-4.

89. Moore, E. B.; Molinero, V., Structural transformation in supercooled water controls the crystallization rate of ice. *Nature* **2011,** *479* (7374), 506-8.

90. Eickhoff, L.; Dreischmeier, K.; Zipori, A.; Sirotinskaya, V.; Adar, C.; Reicher, N.; Braslavsky, I.; Rudich, Y.; Koop, T., Contrasting Behavior of Antifreeze Proteins: Ice Growth Inhibitors and Ice Nucleation Promoters. *J Phys Chem Lett* **2019,** *10* (5), 966-972.

91. Charpentier, T. V. J.; Neville, A.; Millner, P.; Hewson, R.; Morina, A., An Investigation of Freezing of Supercooled Water on Anti-Freeze Protein Modified Surfaces. *Journal of Bionic Engineering* **2013,** *10* (2), 139-147.

92. O'Sullivan, D.; Murray, B. J.; Ross, J. F.; Whale, T. F.; Price, H. C.; Atkinson, J. D.; Umo, N. S.; Webb, M. E., The relevance of nanoscale biological fragments for ice nucleation in clouds. *Sci Rep* **2015,** *5*, 8082.

93. M. J. Molina; R. Zhang; P. J. Wooldridge; J. R. McMahon; J. E. Kim; H. Y. Chang; Beyer, K. D., Physical Chemistry of the H2SO4/HNO3/H2O System: Implications for Polar Stratospheric Clouds. *Science* **1993,** *261*.

94. Kreder, M. J.; Alvarenga, J.; Kim, P.; Aizenberg, J., Design of anti-icing surfaces: smooth, textured or slippery? *Nature Reviews Materials* **2016,** *1* (1).

95. A. C. Cuthbertson; Maass, O., Hydrogen Peroxide. VII. The Dielectric Constants, Refractive Indices and Ionizing Power of Hydrogen Peroxide and Its Aqueous Solutions. *J. Am. Chem. Soc.* **1930,** *52*.

96. Linton, E. P.; Maass, O., THE DIELECTRIC CONSTANTS OF HYDROGEN PEROXIDE-ETHER AND HYDROGEN PEROXIDE-WATER-ETHER MIXTURES. *Canadian journal of research* **1931,** *4*.

97. Gross, P. M.; Taylor, R. C., The Dielectric Constants of Water, Hydrogen Peroxide and Hydrogen Peroxide—Water Mixtures1,2. *Journal of the American Chemical Society* **1950,** *72* (5), 2075-2080.

98. Miller, R. L.; Hornig, D. F., Infrared Spectrum and Force Field of Crystalline Hydrogen Peroxide. *The Journal of Chemical Physics* **1961,** *34* (1), 265-272.

99. Arnau, J. L.; Giguere, P. A., Vibrational spectra and normal coordinate analysis of crystalline H2O2, D2O2 and HDO2. *spectrochimica Acta* **1974,** *30A*, 777-796.

100. Taylor, R. C.; Cross, P. C., Raman Spectra of Hydrogen Peroxide in Condensed Phases. I. The Spectra of the Pure Liquid and Its Aqueous Solutions. *J Chem Phys* **1956,** *24* (1), 41-44.

101. Giguère, P. A., The Infra-Red Spectrum of Hydrogen Peroxide. *The Journal of Chemical Physics* **1950,** *18* (1), 88-92.

102. Moin, S. T.; Hofer, T. S.; Randolf, B. R.; Rode, B. M., An ab initio quantum mechanical charge field molecular dynamics simulation of hydrogen peroxide in water. *Computational and Theoretical Chemistry* **2012,** *980*, 15-22.

103. Arunau, J. L.; Giguere, P. A., Etude Spectroscopique des Derives du Peroxyde d-Hydrogene. VI. Le Dihydrate H2O2-2H2O. *Canadian Journal of Spectroscopy* **1972**.

104. Martins-Costa, M. T. C.; Ruiz-López, M. F., Molecular dynamics of hydrogen peroxide in liquid water using a combined quantum/classical force field. *Chemical Physics* **2007,** *332* (2-3), 341-347.

105. Olovsson, I.; Templeton, D. H., The crystal structure of hydrogen peroxide dihydrate. *Acta Chemica Scandinavica* **1960,** *14*.

106. Wu, X.; Lu, W.; Streacker, L. M.; Ashbaugh, H. S.; Ben-Amotz, D., Temperature-Dependent Hydrophobic Crossover Length Scale and Water Tetrahedral Order. *J Phys Chem Lett* **2018,** *9* (5), 1012-1017.

107. Morawietz, T.; Marsalek, O.; Pattenaude, S. R.; Streacker, L. M.; Ben-Amotz, D.; Markland, T. E., The Interplay of Structure and Dynamics in the Raman Spectrum of Liquid Water over the Full Frequency and Temperature Range. *J Phys Chem Lett* **2018,** *9* (4), 851-857.

108. Tomlinson-Phillips, J.; Davis, J.; Ben-Amotz, D.; Spangberg, D.; Pejov, L.; Hermansson, K., Structure and dynamics of water dangling OH bonds in hydrophobic hydration shells. Comparison of simulation and experiment. *J Phys Chem A* **2011,** *115* (23), 6177-83.

109. Morawietz, T.; Urbina, A. S.; Wise, P. K.; Wu, X.; Lu, W.; Ben-Amotz, D.; Markland, T. E., Hiding in the Crowd: Spectral Signatures of Overcoordinated Hydrogen-Bond Environments. *J Phys Chem Lett* **2019,** *10* (20), 6067-6073.

110. Charles E. Huckaba; Keyes, F. G., The Density of Aqueous Hydrogen Peroxide Solutions. *J. Am. Chem. Soc.* **1948,** *70* (7).

111. Ayumi Minoguchi; Ranko Richert; Angell, C. A., Dielectric Relaxation in Aqueous Solutions of Hydrazine and Hydrogen Peroxide: Water Structure Implications. *J. Phys. Chem. B* **2004,** *108*.

VITA

Aria J. Bredt was born June 9, 1994 and raised in Richland Washington where she graduated from Hanford High school in 2012. She then graduated cum laude from Case Western Reserve University in Cleveland, Ohio with a Bachelor of Science in Chemistry with Honors in 2016. In 2021, Aria obtained a Doctor of Philosophy in Chemistry from Purdue University in West Lafayette, Indiana.